ELSEVIER

Contents lists available at ScienceDirect

Journal of Infrastructure Intelligence and Resilience

journal homepage: www.journals.elsevier.com/journal-of-infrastructure-intelligence-and-resilience





Strain signal denoising in bridge SHM: A comparative analysis of MODWT and other techniques

Yun-Xia Xia^{a,*}, Ru-Kai Xu^a, Yi-Qing Ni^b, Zu-Quan Jin^a

- ^a School of Civil Engineering, Qingdao University of Technology, Qingdao, China
- ^b Department of Civil and Environmental Engineering, The Hong Kong Polytechnic University, Hung Hom, Hong Kong, China

ARTICLE INFO

Handling Editor: Ms. Yanwei Li

Keywords: Structural health monitoring Denoising Strain signal Wavelet

ABSTRACT

Accurate denoising of strain signals is critical for early damage detection in bridge structural health monitoring (SHM). However, signals denoising methods often struggle with the non-stationary and broadband noise encountered in real-world environments. This study provides the first comprehensive comparison of various denoising techniques specifically tailored for bridge strain signals, emphasizing the maximal overlapping discrete wavelet transform (MODWT) for its capacity to handle complex noise profiles. We rigorously compare MODWT with time-domain (moving average filter, finite impulse response filter, empirical mode decomposition), frequency-domain (bandpass filter, Fourier mode decomposition), and other wavelet-based (discrete wavelet transform) approaches. Uniquely, this study employs three datasets from two distinct bridge types (masonry arch and steel bowstring) and evaluates performance using both expert assessments and quantitative metrics (signal-to-noise ratio, peak signal-to-noise ratio, root mean square error, and correlation coefficient). Our findings demonstrate that MODWT exhibits a distinct advantage in high-intensity white noise environments, a common scenario in real-world bridge monitoring, offering valuable guidance for engineers in selecting appropriate denoising strategies. The results not only validate MODWT as a promising preprocessing technique but also offer critical insights into the limitations of existing methods, paving the way for the development of more adaptive and robust denoising solutions in bridge SHM.

1. Introduction

Bridges are important components of infrastructure, and their safety necessitates reliable structural health monitoring (SHM) (Desjardins and Lau, 2024; Tan et al., 2024; Li et al., 2025). SHM systems typically involve the installation of sensors, such as accelerometers and strain gauges, on bridge components to capture structural responses. Strain measurements provide crucial insights into the local behavior of bridge structures, enabling the early detection of damage, including cracks, corrosion, and material fatigue (Anastasopoulos et al., 2021; Hu et al., 2017; Huang et al., 2020; Mao et al., 2019). However, strain signals are often contaminated by various noises, which can distort the signals and diminish the reliability of damage detection and condition assessment. The noise in strain measurements typically originates from intrinsic working principles, operational systems, and external factors (Glišić, 2024; Vaseghi, 2008). Intrinsic sources include thermal noise, flicker noise, and photon shot noise. In resistive strain gauges, system noise mainly arises from amplifiers, analog-to-digital converters, and lead

wire resistance, while fiber optic sensors are affected by Rayleigh and Brillouin scattering. External factors include electromagnetic interference (EMI), temperature fluctuations, and mechanical vibrations.

These noise components generally span a broad frequency range. For instance, flicker noise and long-duration mechanical drifts tend to occur at lower frequencies, while EMI noise often begins around 50–60 Hz (due to power line interference) and extends into the kHz to MHz range for high-speed electronics. Consequently, these noises frequently overlap with structural responses in both frequency and time domains, complicating the isolation of genuine strain responses needed for detecting potential structural damage. In many cases, simple filtering algorithms fail to sufficiently eliminate these noises and may even degrade critical strain signal features. Moreover, the non-stationary nature of both the structural response and noise adds complexity to the denoising process. As ambient conditions, such as traffic, wind, and other operational variables, fluctuate throughout the day or across seasons, both strain signals and unwanted noise can vary unpredictably. Conventional methods designed for stationary signals often

E-mail address: xiayunxia@qut.edu.cn (Y.-X. Xia).

https://doi.org/10.1016/j.iintel.2025.100155

^{*} Corresponding author.

underperform under these evolving conditions.

Researchers have proposed various digital signal denoising techniques (Vaseghi, 2008), a classic problem in signal processing. These methods can generally be categorized into time, frequency, and time-frequency (TF) domain approaches. In the time domain methods, denoising operate directly on the signal samples. Traditional techniques include linear filters such as moving average (MA) filters and finite impulse response (FIR) filters (Blackledge, 2006; Hamming, 1989), as well as nonlinear filters like median filters. MA filters smooth the signal by averaging neighboring samples, while median filters replace each sample with the median of its neighbors, effectively removing impulsive noise while preserving edges. These two filters are straightforward to implement and interpret. Nonetheless, both are sensitive to the filter window size, limiting their tuning capabilities. FIR filters offer greater design flexibility and effective noise reduction but may introduce irregularities in the frequency response if designed for sharp cutoffs.

Time-domain decomposition techniques effectively separate mixed signals into individual components, making them a valuable tool for noise removal in various applications, including mechanical fault diagnosis, audio processing, and biomedical signal analysis (Jiang et al., 2019; Kaur et al., 2021; Kopsinis and McLaughlin, 2009; Massar et al., 2025; Yin et al., 2022). By breaking down complex signals, these methods facilitate the isolation of noise from the desired signal. One prominent example of this approach is empirical mode decomposition (EMD) (Huang et al., 1998) and its derivatives, such as variational mode decomposition (VMD) (Dragomiretskiy and Zosso, 2013). It is a data-adaptive technique that decomposes a signal into intrinsic mode functions (IMFs), which represent simple oscillatory modes with well-defined instantaneous frequencies. In practice, when applied to a noisy signal, EMD can adeptly isolates intrinsic modes that highlight the underlying signal structure while effectively filtering out high-frequency noise. As a result, the original signal can be reconstructed by selectively combining the relevant IMFs and discarding those associated with noise. Another compelling approach to signal decomposition and noise removal is blind source separation (BSS) methods, particularly independent component analysis (ICA) (Comon, 1994). These techniques operate under assumptions that the observed mixed signals comprise non-Gaussian and statistically independent sources. By leveraging higher-order statistical analysis, ICA can effectively recover the original signals from their linear mixtures. This capability is particularly advantageous in scenarios where noise distinguishes itself based on its statistical properties. While the signal decomposition methods have advanced signal denoising applications (Aliouat and Djendi, 2025; Kopsinis and McLaughlin, 2009; Yin et al., 2022), their computational demands can scale significantly with data dimensionality. For instance, the sifting process of EMD has a complexity of $O(N^2)$ (Huang et al., 1998), where *N* is the signal length; and quadratic penalty optimization in VMD requires multiple Fourier transforms per iteration (Dragomiretskiy and Zosso, 2013). Such high computational costs present obstacles for real-time implementation.

In contrast to time-domain techniques, frequency-domain methods offer a different approach to denoising through transforming signals from the time domain into the frequency domain using the Fourier transform (FT) (Oppenheim et al., 1999). This transformation is fundamental, enabling an in-depth analysis of a signal's frequency components. By decomposing the signal into sinusoids, the FT reveals the amplitude and phase of each frequency component, which is essential for characterizing signal properties. Unwanted components, such as noise, can often be removed based on their frequency-domain characteristics, using flexible filtering techniques (Wahab et al., 2021). Frequency-domain methods are particularly effective when the noise and the desired signal occupy distinct frequency bands. However, they are most suited for stationary signals with consistent statistical properties over time and frequency-distinguishable components. Furthermore, converting signals to the frequency domain loses temporal information, posing challenges for analyzing time-varying signals, a prevalent

scenario in bridge SHM.

To address these challenges, researchers often employ hybrid approaches that integrate frequency-domain and time-domain techniques, collectively known as TF methods. These methods simultaneously analyze signals across both domains. Thus, they are particularly effective for signals with time-varying frequency content. Time-frequency representations (TFRs) (Boashash, 2016) such as the short-time Fourier transform (STFT) and wavelet transform (WT), serve as the foundation for many denoising techniques. TFR-based denoising typically employs thresholding techniques, where coefficients below a predefined threshold are suppressed, thereby eliminating noise while preserving important signal features. WT excels at capturing both high- and low-frequency components across multiple scales, making it particularly suitable for analyzing time-varying signals like bridge strain data. There are various WT variants, each designed to meet specific analytical needs. The discrete wavelet transform (DWT) (Sundararajan, 2015), well-regarded for its computational efficiency, is widely applied in preprocessing SHM signals. For instance, Wu et al. (2014), Ni et al. (2012), Zhao et al. (2019), and Wei et al. (2017) have utilized DWT to effectively isolate temperature- or traffic-induced components from strain data. Ma et al. (2024) employed DWT to eliminate noise in vacuum-process monitoring signals of aerospace vacuum vessel structures. However, despite its advantages, DWT has notable limitations, such as issues associated with downsampling and boundary management (Daubechies, 1992; Strang and Nguyen, 1996).

The maximal overlapping discrete wavelet transform (MODWT) (Percival and Walden, 2000), an advanced variant of the traditional DWT, offers a refined approach to analyzing TF characteristics in signals. One of MODWT's outstanding features is its avoidance of downsampling during transformation, which preserves all data points and significantly enhances the resolution of both global and local signal features. This capability makes MODWT particularly valuable for applications requiring precise signal reconstruction. Notably, MODWT has demonstrated promising results in processing complex and non-stationary signals across diverse fields (Barzegar et al., 2021; Li et al., 2014; Osmani et al., 2024; Patel et al., 2014), including finance, healthcare, and engineering. For example, in biomedical signal processing (Kumar et al., 2021), MODWT has significantly improved electrocardiogram denoising, leading to enhanced accuracy in heart rate variability analysis. Recently, Xia et al. (2024) developed a novel MODWT-based filter, highlighting its efficacy in denoising applications for bridge SHM.

Each denoising method discussed above presents its own strengths and limitations, with effectiveness highly dependent on the signal characteristics and noise types encountered in real-world applications. In the field of bridge SHM, denoising strain signals remains challenging due to non-stationary, broadband noise from diverse sources. Currently, most studies focus on optimizing individual methods (Jiang et al., 2022), offering depth but often lacking comprehensive comparisons. Limited comparative studies exist; for example, Deng et al. (2023) compared wavelet, mathematical morphology, and low-pass filtering methods for cable force monitoring. While these studies provide valuable insights, no research has yet comprehensively and systematically compared multiple denoising methods using unified datasets that account for diverse bridge types and varying noise levels or thoroughly analyzed performance in non-stationary, broadband noise environments. This gap emphasizes the need for a more holistic understanding of optimal denoising strategies, suggesting that future research should integrate existing methods with standardized datasets to develop more reliable and effective preprocessing tools for bridge SHM.

In this study, we introduce a systematic approach for selecting the most suitable denoising algorithms for complex strain signals specific to bridge SHM. We analyzed seven representative methods: three time-domain techniques (MA filter, FIR filter, and EMD), two frequency-domain approaches (bandpass filter, and frequency mode decomposition), and two TF methods (DWT and MODWT). The selection of the

seven denoising methods was driven by their widespread use in bridge SHM applications. These methods represent a broad spectrum of traditional approaches, providing a robust baseline. While modern techniques, such as deep learning-based denoising (Tian et al., 2020; Yu et al., 2019) and adaptive filtering, show promise in certain contexts, they often require large training datasets, extensive computational resources, or specific assumptions about noise characteristics, which may not align with the practical constraints of real-world bridge SHM systems, where data availability and computational efficiency are critical. Our study focuses on methods that are readily implementable in current SHM frameworks, ensuring immediate applicability for engineers. Nonetheless, we recognize the potential of emerging techniques and plan to investigate their applicability in future studies.

To ensure fair comparisons, we ensured that each denoising method was optimized for performance. We utilized grid search (Liashchynskyi and Liashchynskyi, 2019) to determine the most effective hyperparameters for each technique. The denoising performance of these methods was evaluated using both qualitative and quantitative assessments. Qualitative evaluations were conducted by experts to confirm that the denoised outputs resonated well with human perception. On the other hand, quantitative assessments employed four metrics: signal-to-noise ratio (SNR), peak signal-to-noise ratio (PSNR), root-mean-square error (RMSE), and correlation coefficient (CC). The results indicated that the MODWT-based algorithm consistently produced outputs with superior visual quality. In addition, it excelled across all performance metrics, effectively balancing noise reduction with the preservation of critical signal features.

The remainder of this paper is organized as follows. Section 2 provides a review of existing denoising techniques for digital signals. Section 3 outlines the methodology of this comparative study, including the procedure, datasets, selected methods for comparison, and performance metrics. Section 4 presents the results, along with discussions. Finally, Section 5 concludes the paper and outlines directions for future work.

2. Existing denoising techniques for digital signals

The removal of noise, defined as unwanted disturbances that obscure meaningful information, is a critical research area in digital signal processing. Depending on the operational domain, denoising techniques can be categorized into time-domain, frequency-domain, and time-frequency TF domain approaches. Below, we review several representative denoising methods, highlighting their underlying principles and performance across diverse contexts.

2.1. Time-domain methods

2.1.1. Digital filters

Time-domain methods operate directly on signals in their original time representation. Among these methods, digital filters (Hamming, 1989), encompassing linear filters such as MA and FIR filters, as well as nonlinear filters like median filters (Pitas and Venetsanopoulos, 1990), have long served as foundational tools for signal denoising.

The MA filter smooths the signal by averaging a specified number of adjacent samples, thereby reducing rapid fluctuations caused by noise. Mathematically, it can be written as:

$$y(n) = \frac{1}{M} \sum_{m=0}^{M-1} x(n-m), \tag{1}$$

where x(n) is the discrete input signal, y(n) is the output signal, M is the window size of the moving average filter. Its performance depends heavily on the choice of window size M. Although a larger M provides more noise attenuation, it can blur sharp features, while a smaller M better preserves detail but may result in less noise reduction.

Finite impulse response (FIR) filters, offer a more flexible framework for digital signal denoising than the moving average approach. It operates by convolving the input signal with a finite sequence of coefficients which define the filter's behavior (Oppenheim et al., 1999):

$$y(n) = \sum_{m=0}^{M-1} h(m)x(n-m),$$
 (2)

where h(m) is the impulse response of the filter, which is designed using the filter order M and a cutoff frequency, f_c ; x(n-m) represents the delayed input samples. To ensure zero-phase filtering, forward and reverse filtering techniques can be employed to effectively mitigate phase distortion and keep the original timing of the signal intact. That is,

$$y(n) = \sum_{m=0}^{M-1} h(m)[x(n-m) + x(n+m)].$$
 (3)

The output signal y(n) is computed as a weighted sum of the current and past input values, with the weights determined by the filter coefficients.

The impulse response of the filter h(m) can be expressed as

$$h(m) = \sum_{k=0}^{M-1} a_k \cdot w(m-k), \tag{4}$$

where a_k are the coefficients for the desired frequency response, w(n-k) is the window function used, e.g., Hamming window or Hanning window. The ideal frequency response of an FIR filter is

$$H(e^{j\omega}) = \begin{cases} 1 & 0 \le |\omega| < \omega_c \\ 0 & \text{otherwise} \end{cases}$$
(5)

where ω_c is the cutoff angular frequency, $H(e^{j\omega})$ is the frequency response of the filter, and $\omega = 2\pi f$. Unlike MA filters, where the weights are all equal, the FIR filter allows for varying coefficients that can optimize different performance criteria, such as rapid roll-off in the frequency domain.

2.1.2. Time-domain decomposition method

Time-domain decomposition techniques are powerful methods for separating a mixed signal into its individual components, providing an effective means of eliminating noise in digital signals. These methods are especially effective for nonstationary signals, where traditional frequency-domain techniques may struggle. Two prominent approaches in this category are EMD and BSS, which can also be considered as two families of methods.

EMD is a data-driven technique that decomposes a signal decomposes a signal x(t) into amplitude- and frequency-modulated components called intrinsic mode functions (IMFs) and a residual r(t) (Huang et al., 1998):

$$x(t) = \sum_{i=1}^{L} IMF_i(t) + r(t), \tag{6}$$

where L is the total number of IMFs. Each IMF satisfies two conditions: (1) The number of extrema and zero crossings must either be equal or differ by at most one; and (2) the mean value of the envelope defined by the local maxima and minima is zero. Many adaptive methods like VMD (Dragomiretskiy and Zosso, 2013) have been developed based on EMD.

In the context of denoising, EMD can be used to separate noise from the signal by identifying and removing IMFs that primarily contain noise. For example, high-frequency IMFs often correspond to noise. Then a denoised signal y(t) can be reconstructed by summing only the relevant IMFs:

$$y(t) = \sum_{i=l_c}^{L} IMF_i(t), \tag{7}$$

where l_c is the cutoff level, or the index of the first IMF deemed to

contain meaningful signal information.

BSS is a family of techniques that separate mixed signals based on their statistical properties rather than their oscillatory characteristics. Suppose we have observed signals represented by the vector $\mathbf{x}(t) = (x_1(t), x_2(t), ..., x_p(t))^T$, where p is the number of measurement channels and t indexes time. These signals are created by mixing original sources $\mathbf{s}(t) = (s_1(t), s_2(t), ..., s_n(t))^T$ using a mixing matrix \mathbf{A} , with added noise $\mathbf{n}(t)$ (Cardoso, 1998):

$$\mathbf{x}(t) = \mathbf{A}\mathbf{s}(t) + \mathbf{n}(t) \tag{8}$$

Recovering the sources means estimating both \boldsymbol{A} and $\boldsymbol{s}(t)$, which is challenging because both are unknown. A popular BSS method is ICA (Hyvärinen et al., 2009), which assumes that the source signals are statistically independent. By maximizing independence, ICA identifies a separating matrix \boldsymbol{W} such that

$$\widehat{\boldsymbol{s}}(t) = \boldsymbol{W}\boldsymbol{x}(t),\tag{9}$$

where $\hat{s}(t)$ is the estimated version of s(t). If the noise n(t) is not too strong and the signals are non-Gaussian and independent, ICA can effectively denoise the signals.

While time-domain decomposition methods like EMD and BSS are powerful, they can be computationally intensive. For example, EMD involves iterative sifting, which can be slow for long signals or high sampling rates. ICA requires optimization routines to maximize statistical independence, which can be time-consuming for large datasets. Additionally, BSS techniques typically require multi-channel data, limiting their applicability to single-channel signals.

Given that ICA necessitates multi-channel data and assumes that the signal sources are non-Gaussian and independent, this study does not utilize this method as a comparative approach. The focus of this study is on denoising single-channel signals, where the signal components may not readily satisfy the non-Gaussian condition.

2.2. Frequency-domain methods

Frequency-domain methods perform digital signal denoising by isolating specific frequency components. Rather than operating in the time domain, where signals can appear convoluted or overlapping, frequency-domain methods convert signals into representations that clearly show which frequency bands contain noise or meaningful information. This transformation allows us to selectively reduce noise in the frequency domain.

The foundation of frequency-domain analysis is the discrete Fourier transform (DFT) (Oppenheim et al., 1999). For a discrete signal x(n) of length N, the DFT is given by

$$X(k) = \sum_{n=0}^{N-1} x(n)e^{-\frac{2\pi}{N}kn}, k = 0, 1, ..., N-1,$$
(10)

where X(k) represents the signal in the frequency domain, and k indexes the frequency bins. This transformation reveals how different frequencies contribute to the original signal. It enables targeted noise reduction through filtering. By analyzing the magnitudes and phases of X(k), specific frequency components associated with noise can be identified and selectively attenuated. Once the unwanted components are reduced or eliminated, the signal can be reconstructed using the inverse discrete Fourier transform (IDFT)

$$x(n) = \frac{1}{N} \sum_{k=0}^{N-1} X(k) e^{\frac{2\pi}{N}kn}$$
 (11)

This process effectively converts the filtered signal back to its original time-domain representation, preserving the essential features while minimizing noise.

One particularly effective method for noise reduction in the time domain is frequency bandpass (FB) filtering (Proakis and Manolakis,

2021). This technique permits only a specific range of frequencies, defined by a lower frequency f_{min} and an upper frequency f_{max} , to pass through while attenuating frequencies outside this range. The filtering process can be expressed as follows:

$$X_{\text{filtered}}(k) = \begin{cases} X(k) & \text{if } f_{\min} \le f_k \le f_{\max} \\ 0 & \text{otherwise} \end{cases}, \tag{12}$$

where f_k represents the frequency corresponding to the kth Fourier coefficient. By selectively retaining frequencies within the desired range, FB filtering removes noise components that lie outside the band of interest. This method is particularly advantageous due to its straightforward implementation, flexibility in adjusting frequency parameters, and precise control over noise reduction.

For a more nuanced approach, frequency mode decomposition (FMD) can be employed. FMD represents a signal as a sum of distinct frequency modes, each characterized by its angular frequency ω_l and a complex coefficient α_l (Oppenheim et al., 1997):

$$x(n) = \sum_{l=1}^{L} \alpha_l e^{j\omega_l n}, \tag{13}$$

where L is the number of frequency modes.

The Fourier coefficients X(k) can be viewed as a form of α_l (Bracewell, 2000), revealing the distribution of the signal's energy across different frequencies. The amplitude spectrum A(k) and the phase spectrum $\varphi(k)$ are derived from X(k) as follows:

$$A(k) = |X(k)|, \varphi(k) = \arg(X(k)). \tag{14}$$

FMD allows for the selective filtering of frequency modes based on their energy contributions, facilitating noise reduction. Modes dominated by noise, typically characterized by low energy or irregular frequency patterns, can be identified and suppressed.

In this study, a dynamic thresholding approach was utilized to distinguish signal components from noise. The noise threshold was determined using the amplitude spectrum A(k), and statistical measures such as the median and standard deviation:

$$\tau = \operatorname{meadian}(A(k)) + p \cdot \sigma_{A(k)}, \tag{15}$$

where p is a user-defined parameter that controls the sensitivity of noise detection.

Filtering in the frequency domain can be straightforward, particularly when noise is concentrated in specific frequency bands. As a result, Fourier-based techniques work well for stationary signals, where noise characteristics stay mostly the same over time.

2.3. TF methods

TF methods build on traditional time- or frequency-domain techniques by combining both perspectives into one framework. This dual approach gives a detailed view of signal characteristics across time and frequency. It is especially useful for signals that change over time. Wavelet-based thresholding is a popular technique because it is simple and effective. It decomposes a signal into coarse and fine components. This facilitates targeted noise reduction while preserving important structures in the original waveform.

To process digital signals like those studied in this paper, a common approach begins by applying the DWT to a finite-length signal x(n). At each decomposition level j, the DWT produces an approximation coefficient $a_{j,k}$ and a detail coefficient $d_{j,k}$. This is typically conducted through filter-bank operations. For each level j, these can be written as (Sundararajan, 2015)

$$a_{j,k} = \sum_{n=0}^{N-1} x(n)\phi_{j,k}(n), d_{j,k} = \sum_{n=0}^{N-1} x(n)\psi_{j,k}(n),$$
(16)

where $\phi_{j,k}(n)$ is the scaling function, and $\psi_{j,k}(n)$ is the wavelet function. Both are at scale 2^j and translation k. These functions are defined as:

$$\phi_{ik}(n) = 2^{-j/2}\phi(2^{-j}n - k) \quad \psi_{ik}(n) = 2^{-j/2}\psi(2^{-j}n - k). \tag{17}$$

The scaling function $\phi_{j,k}(n)$ obtains coarse or low-frequency information, while the wavelet function $\psi_{j,k}(n)$ captures fine or high-frequency details.

Once the coefficients are obtained, thresholding helps isolate and remove noise-dominated components. A widely used thresholding rule is soft thresholding. Let λ be the threshold value, then the transformed detail coefficients \hat{d}_{ik} become (Donoho and Johnstone, 1994)

$$\widehat{d}_{j}(k) = \begin{cases} \operatorname{sgn}(d_{j}(k)) (|d_{j}(k)| - \lambda) & \text{if } |d_{j}(k)| \geq \lambda, \\ 0 & \text{otherwise.} \end{cases}$$
(18)

This approach shrinks coefficients that appear to be contaminated by noise while retaining those that likely represent the true signal structure. The threshold parameter λ is typically determined using the universal threshold principle:

$$\lambda = \sigma \sqrt{2 \log N} \tag{19}$$

where σ represents the noise standard deviation, often estimated from the median absolute deviation of the finest-scale wavelet coefficients.

Despite its usefulness, the traditional DWT incorporates down-sampling at each level of decomposition, potentially resulting in the loss of critical information. Its non-overlapping nature and reduced data points may obscure local characteristics within the signal. Furthermore, the DWT can introduce artifacts and distortions at the boundaries of finite-length signals due to the inherent assumptions made during wavelet decomposition.

In contrast, MODWT addresses these limitations by eliminating the decimation step, thereby ensuring shift invariance and retaining the full temporal resolution of the original signal. This property is a significant advantage over traditional DWT, as it prevents the loss of data points and maintains alignment between the wavelet coefficients and the original time series. For bridge SHM applications, where strain signals are often non-stationary and exhibit abrupt changes due to dynamic loading, environmental effects, or structural anomalies, this property is critical. It ensures that subtle temporal features, such as sudden strain spikes or transient responses due to traffic, are not distorted or misaligned during decomposition.

For a given signal x(n), the MODWT coefficients at level j are computed as follows (Strang and Nguyen, 1996):

$$W_{j}(n) = \sum_{l=0}^{L_{f}-1} \widetilde{h}_{j}(l)x(n-l), V_{j}(n) = \sum_{l=0}^{L_{f}-1} \widetilde{g}_{j}(l)x(n-l),$$
 (20)

where $h_i(l)$ and $\tilde{g}_i(l)$ are the MODWT scaling and wavelet filters, respectively, and L_f is the filter length. These filters are designed to capture both low-frequency trends (scaling coefficients) and highfrequency details (wavelet coefficients) in the signal. Unlike the traditional DWT, MODWT does not discard samples between decomposition levels, resulting in a redundant representation that preserves all time points. This redundancy enhances its robustness when analyzing complex signals, such as those with significant noise, or abrupt variations, which are common characteristics of bridge strain data under operational conditions. In the context of bridge strain denoising, MODWT provides a higher resolution of detail coefficients at each decomposition level by avoiding downsampling, improving the separation of noise from meaningful signal features. This enhances denoising performance, as noise-dominated coefficients can be more effectively isolated and suppressed without compromising the integrity of low-amplitude structural responses. In addition, MODWT reduces boundary distortions, a common issue in DWT when processing finite-length bridge strain records,

ensuring that edge effects do not obscure critical information near the signal boundaries. These improvements make MODWT well-suited for denoising bridge strain signals, where maintaining signal fidelity and capturing subtle, time-varying features are paramount for reliable structural assessment.

3. Methodology

3.1. Procedure

The flowchart in Fig. 1 illustrates the procedure of this comparative study. The acquisition of strain datasets is the initial and essential step. Once the datasets are available, noise is introduced into the signals to generate noisy signals that simulate real-world challenges. These synthesized noisy signals serve as the benchmark for evaluating the denoising methods. Subsequently, parameters for the benchmark signals, including the SNR and PSNR, are calculated. Various methods are then applied to clean the noisy strain signal. After denoising, the performance of these techniques is compared to identify the most effective methods for reducing noise while maintaining signal integrity.

3.2. Datasets

This study uses three strain datasets. Signals in each dataset represent a distinct strain pattern. The datasets are publicly available (Alexakis et al., 2021; Maes and Lombaert, 2020) and are described below.

Dataset 1 is drawn from the Marsh Lane Bridge, an arch-type railway structure in the UK built between 1865 and 1869. This bridge carries

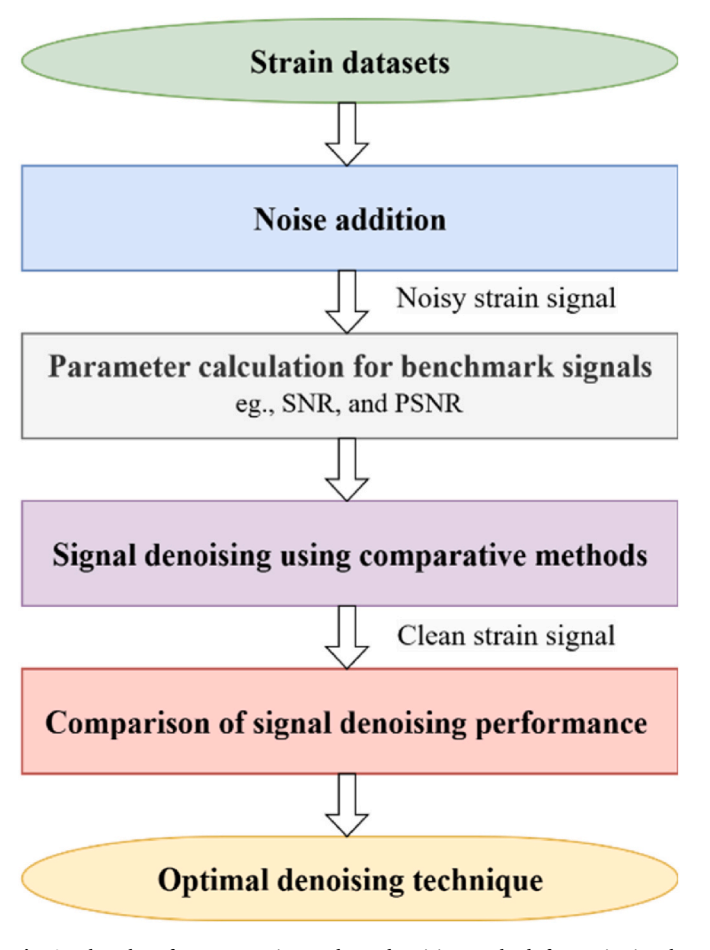


Fig. 1. Flowchart for comparative study on denoising methods for strain signals in bridge SHM.

two electrified tracks and currently accommodates over 200 trains per day. Prolonged exposure to environmental factors coupled with increasingly heavy train loads led to notable damage. Consequently, in 2015 the bridge underwent repairs, involving concrete infilling of the pier relieving arches and the installation of steel ties to control transverse movements of both the piers and the spandrel walls. The most serious damage centers on the relieving arches located mid-pier, where a spreading mechanism causes the keystone to drop and the pier walls to bow outward. The pier between Arches 37 and 38 is surrounded by transverse cracks, resulting from the pronounced out-of-plane rocking response under train loads prior to the 2015 intervention. Longitudinally, separation cracks were found between the spandrel walls and arch barrels of Arches 37 and 38, and a longitudinal crack developed beneath the north track of Arch 37.

In July 2016, only a few months after the repair, a network of FBG strain sensors was installed beneath Arches 37 and 38 to capture detailed dynamic deformations. Then, in November 2017, this temporary setup was superseded by a permanent FBG monitoring system beneath Arches 37, 38, and 39, designed to evaluate the long-term effectiveness of the 2015 retrofit and monitor ongoing structural health (Alexakis et al., 2021). The FBG network comprises 47 longitudinal and 17 transverse strain sensors, 4 sensors on steel wires connecting the springs of Arches 37 and 39 (beneath the longitudinal strain arrays) to record changes in arch span, and 5 temperature sensors. Data collection relies on a four-channel sm130 Optical Sensing Interrogator (Micron Optics, Inc.), which can sample each sensor at 1 kHz with a resolution of ± 2 micro-strain ($\mu \varepsilon$). Each of the four channels is connected to a fiber optic cable carrying 20 FBG sensors, totaling 80. The cables are pre-tensioned, with each grating clamped to measure strain over approximately 1 m between two fixed points. A data logger triggers acquisition upon train passages, and the measurements are transmitted via 4G to the University of Cambridge.

The strain signals in Dataset 1 were collected from the FBG sensors labeled 37NA3A4 and 37NA6A7 on Arch #37, oriented along the longitudinal direction of the arch. This dataset contains 257 fragments of transient dynamic strain variations recorded during train passages. In this study, we focus solely on the transient dynamic strain due to passing trains. Within such a brief time window, temperature-induced wavelength variations are considered negligible.

Datasets 2 and 3 were collected from the KW51 railway bridge in Belgium, a bowstring arch structure measuring 115 m in length and 12.4 m in width. The bridge accommodates two ballasted, electrified tracks (Track A on the north side and Track B on the south side) with a maximum operational speed of 160 km/h. Both tracks are curved, featuring radius of 1125 m for Track A and 1121 m for Track B. The bridge, primarily used by passenger trains, opened for service in 2003 and has been monitored since October 2, 2018. Between May 15 and September 27, 2019, it underwent retrofitting to correct a construction issue identified during inspection, which involved welding steel boxes around the original bolted connections where the diagonals meet the arches and the bridge deck.

Strains on the deck and diagonals are measured via 12 uniaxial Micro-Measurements CEA-06-250UN-350 strain gauges (nominal resistance RG = 350 Ω) (Maes and Lombaert, 2021). Of these, eight are installed on the bridge deck to capture longitudinal strain in the main girders; they are placed near midspan between consecutive transverse beams, and their channels are labeled with the format sgBD α 1 α 1 α 2 α 2 β δ . The remaining four gauges measure axial strain (dominated by axial force and bending) in two diagonals connecting to the bridge deck at measurement lines 20 and 23 on the south side (leaning toward Leuven). Each gauge is positioned on a rectangular-section diagonal profile, 85 cm from the bottom.

All gauges utilize a quarter-bridge Wheatstone configuration with an NI 9237 module providing bridge completion, data acquisition, signal conditioning, and a 5 V excitation source. A physical resistor of R3 = 350 Ω is added for bridge balancing. The NI 9237 features an A/D range

of ± 25 mV/V and a 24-bit resolution. LabVIEW converts the measured output voltage into strain (ϵ) using the nominal gauge parameters (gauge factor $k=2.16,\ RG=350\ \Omega)$ and the lead wire resistance RL measured during installation. Positive strain indicates tension, while negative strain denotes compression. Each gauge is protected with a Micro-Measurements M-Coat F coating. Data sampling is performed at 1651.6 Hz, followed by decimation by a factor of two, then processed with an eighth-order Chebyshev Type I lowpass filter at 16 Hz (0.1 dB passband ripple), applied in both forward and reverse directions to remove high-frequency noise. Lastly, the signals are shifted so that the first sample of each event corresponds to zero strain.

Dataset 2 includes data from strain gauges labeled sgBD1011A, sgBD1718A, and sgBD1718C, located on opposite sides of the bridge deck, which measure the longitudinal strains in the main bridge girders. In contrast, Dataset 3 was collected from two strain gauges labeled sgDI20ALB and sgDI23ALL, installed on two diagonal members. Similar to Dataset 1, signals in Datasets 2 and 3 also reflect transient dynamic strain variations during a train's passage, comprising 234 and 307 recordings, respectively.

Further details regarding the sensors and data in the three datasets can be found in (Alexakis et al., 2021; Maes and Lombaert, 2021). This paper primarily focuses on the strain patterns associated with the static effects of vehicles. To facilitate this analysis, we preprocessed the raw data using low-pass filters. It is important to note that this filtering does not imply that high-frequency components are uninformative; rather, the dynamic responses of the bridge structures are retained within those components.

Fig. 2(a)–(c) display samples of the strain signals from Datasets 1 to 3, respectively. Negative values indicate contraction, while positive values indicate expansion. It is evident that the passage of each train elicits a distinct response signature. The number of peaks corresponds directly to the number of cars in the train. For instance, in the signals from Dataset 1 (the first row in Fig. 2), the first positive peak marks the moment when the first bogie passes above the sensor, while the last positive peak corresponds to the passage of the last bogie. The intermediate double peaks indicate the passage of intermediate pairs of bogies. The duration of signal fluctuations correlates with the speed of the trains.

There are significant differences in signal patterns among the three datasets. The strain from Dataset 1 oscillates around a value of zero, whereas the signal from Dataset 2 fluctuates around a positive value. This discrepancy is primarily attributed to the differences in bridge lengths. The Marsh Lane Bridge associated with Dataset 1 measures 7.7 m in length, while the KW51 Bridge corresponding to Dataset 2 is 115 m long. Consequently, when a train passes over the Marsh Lane Bridge, it is unlikely for the entire train to be on the arch simultaneously, as the wheels load the arch one by one. In contrast, the KW51 Bridge can accommodate the entire length of a train, resulting in an offset in the strain oscillation due to the overall weight of the train.

Although Datasets 2 and 3 were obtained from the same bridge, their strain signals exhibit notable differences. A significant distinction is that the signal from Dataset 3 displays cycles of both positive and negative values, whereas the signal from Dataset 2 predominantly resides in the positive range. This variation arises from the fact that the signals were collected from different structural components. As mentioned earlier, Dataset 2 was recorded from the main bridge girders, specifically the ties of a bowstring bridge, while Dataset 3 was measured from the diagonals connecting the deck to the arches. When a train traverses the bridge, particularly when a substantial portion of it is on the structure, the ties are tense, whereas the diagonals experience cycles of tension and compression as the gravity center of the train moves across the bridge.

The various shapes of strain signals indicate the temporal and spectral complexity of these signals. To establish a data benchmark for comparative studies, we utilized these preprocessed strain signals as clean signal $x_0(n)$ and added Gaussian white noise $x_{\text{noise}}(n)$ at varying intensities. The resulting noisy signal x(n) is defined by the following

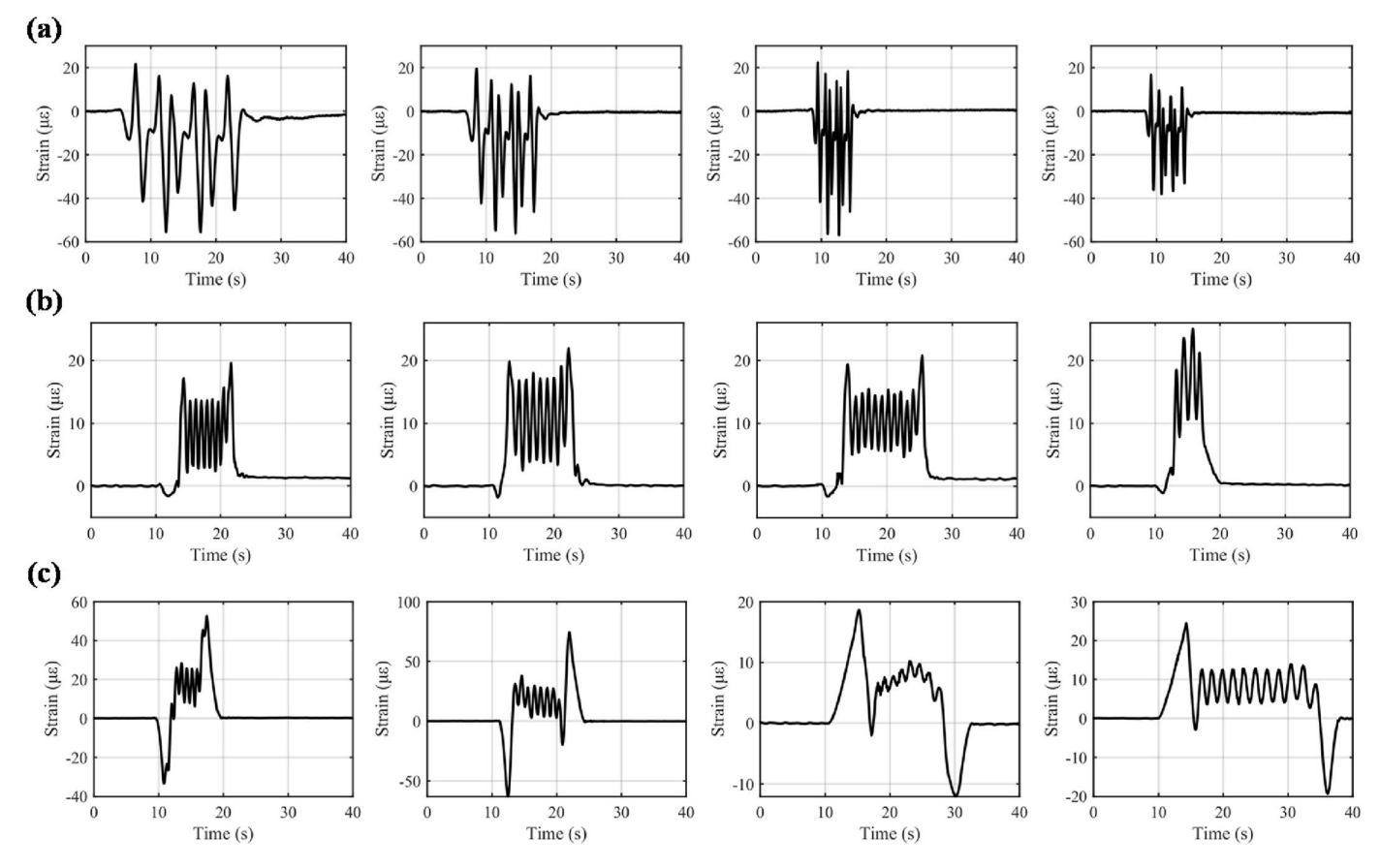


Fig. 2. Signal samples from the three datasets: (a) Dataset 1, (b) Dataset 2, and (c) Dataset 3.

equation:

$$x(n) = x_0(n) + x_{\text{noise}}(n) = x_0(n) + I \cdot \sigma_{x0} \cdot N(0, 1).$$
 (21)

In this expression, I is a predefined noise intensity factor, taking values of 0.1, 0.5, 1, and 3; σ_{x0} represents the standard deviation of $x_0(n)$; and N (0,1) denotes a standard normal distribution. The data used in this study is summarized in Table 1, where the data corresponding to a noise intensity factor of 0 represents the original signal.

We employ the Gaussian white noise because of its well-established utility as a rigorous and standardized noise model in signal processing research. Its uniform power spectral density and lack of temporal correlation mean it overlaps with the signal in both time and frequency

Table 1 Information of data used in this study.

Dataset	Data source	Sensor tag	Number of original signals	Sampling rate (Hz)	Noise intensity factor, <i>I</i>
1	Marsh	37NA3A4	257	1000	0
	Lane	37NA6A7			0.1
	Bridge				0.5
					1
					3
2	KW51	sgBD1011A	234	825.8	0
	Bridge	sgBD1718A			0.1
		sgBD1718C			0.5
					1
					3
3	KW51	sgDI20ALB	307	825.8	0
	Bridge	sgDI23ALL			0.1
					0.5
					1
					3

domains, making it particularly hard to filter out. Consequently, it provides a rigorous test for denoising methods. Furthermore, the Gaussian nature of the noise reflects the cumulative effect of many small, independent disturbances, which is a simplified yet relevant model for real-world noise in strain signals. By varying the noise intensity factor *I*, we can systematically explore the performance limits of the compared denoising methods under progressively harsher conditions. This controlled setup thus serves as a foundational step for the comparative study of strain signal denoising methods before extending it to more complex, real-world noise scenarios.

Taking the data from the second column of Fig. 2 as an example, the resulting noisy signals with varying intensities of Gaussian white noise are illustrated in Fig. 3. It can be seen that the original signals gradually become obscured by the noise, making the details of the signal patterns difficult to discern as I increases, particularly beyond a value of 1. Moreover, the added noise also overlaps with the original signals in the frequency spectrum, as shown in Fig. 4. The presence of noise in both the time and frequency domains poses a significant challenge for signal denoising.

3.3. Compared methods

After a comprehensive review of existing signal denoising approaches in Section 2, we selected seven representative methods to denoise the strain signals across the three datasets. These include three time-domain methods, two frequency-domain methods, and two TF-domain methods. The time-domain methods are the MA filter, FIR filter, and EMD. The frequency-domain methods include the FB filter and FMD. And the TF methods refer to the DWT- and MODWT thresholding methods.

To ensure a fair comparison, it is essential that each method achieves optimal performance when analyzing the same data. This study uses

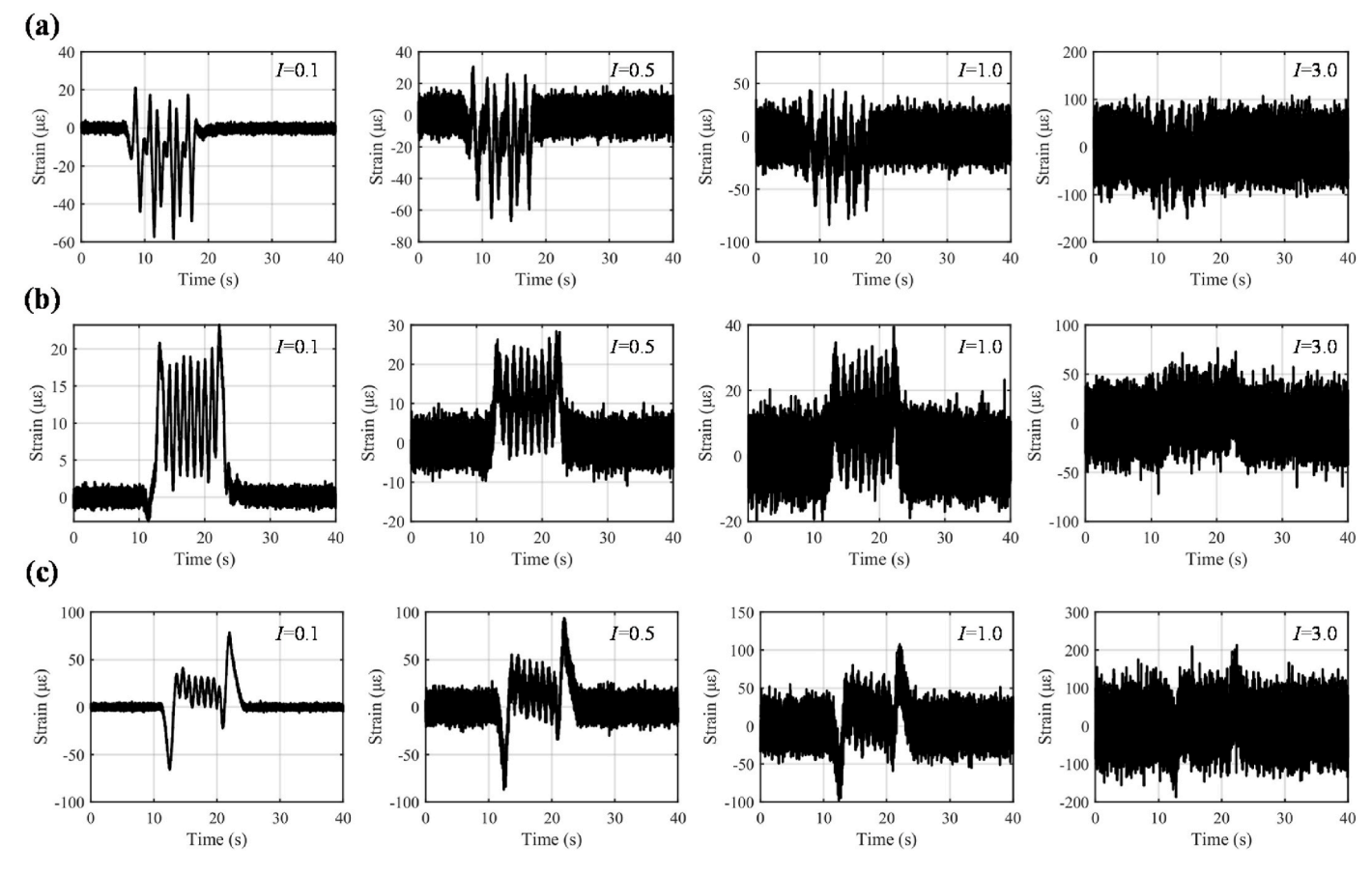


Fig. 3. Samples of noisy signals generated from: (a) Dataset 1, (b) Dataset 2, and (c) Dataset 3.

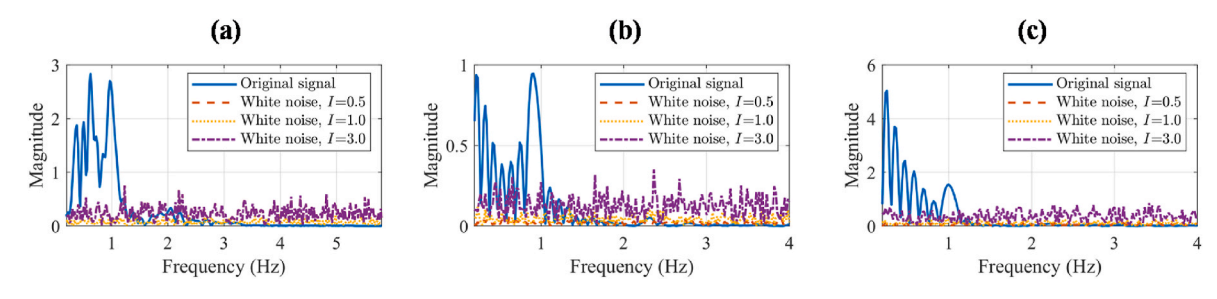


Fig. 4. Frequency spectra of original signals and added noises: (a) Dataset 1, (b) Dataset 2, and (c) Dataset 3.

SNR as a quantitative measure and employes grid search (Xia et al., 2024) to identify optimal hyperparameters for each technique. The search ranges and step sizes for these hyperparameters are detailed in

Table 2. In this table, J_1 and J_2 denote the decomposition levels of DWT and MODWT, respectively. the minimum frequency (f_{min}) is set to 0 Hz across all datasets. Other symbols are defined in Section 2 and remain

Table 2Search ranges and step sizes for denoising hyperparameters.

Dataset	Noisy data (I)	$MA(M_1)$	FIR (f_c)	EMD (l_c)	FB (f_{max})	FMD (<i>p</i>)	DWT (J_1)	MODWT (J_2)
1	0.1	10:10:100	15:1:20	2:1:8	4:0.2:8	0.1:0.1:1	4:1:9	4:1:9
0.5	50:10:200	12:1:18		4:0.2:8	0.4:0.2:2			
	1	80:10:240	4:0.5:6		3:0.2:6	1:0.2:3		
	3	100:20:300	3:0.5:5		2:0.2:4	2:0.5:5		
2	0.1	10:10:100	0.1:0.5:5	2:1:8	5:0.2:7	0.1:0.1:1	5:1:9	5:1:9
	0.5	80:10:200	0.1:0.5:5		1:0.2:4	0.4:0.2:3		
	1	100:10:240	3:0.1:4.5		1:0.2:3	1:0.5:4		
	3	200:10:400	2:0.5:5		1:0.2:2	1:0.5:6		
3	0.1	10:10:100	10:0.2:14	2:1:8	4:0.2:6	0.1:0.1:1	5:1:9	5:1:9
	0.5	80:10:240	4:0.1:5		1:0.2:3	0.4:0.2:2		
	1	100:10:300	3:0.1:4		1:0.2:3	1.1:0.5:4		
	3	260:10:500	1.2:0.2:3		1:0.2:3	2:0.5:6		

consistent throughout. In both DWT and MODWT thresholding, the db4 wavelet basis is selected for its ideal balance of compactness and smoothness, making it especially suitable for capturing the non-stationary characteristics of bridge strain signals. The thresholding strategy employed soft thresholding with a universal threshold. These choices were optimized through preliminary experiments to maximize denoising performance while preserving signal features. Taking signals with noise intensities of 3 in Dataset 3 as an example, Fig. 5 illustrates how the average SNR varies within the search range for each denoising method. The optimal parameters for the seven compared denoising methods are presented in Table 3.

3.4. Performance metrics

The performance of the seven denoising methods was evaluated both qualitatively and quantitatively. First, experts assessed the effectiveness of signal denoising by visually analyzing waveform graphs. They checked if noise was removed while keeping the critical features of the original signal. Subsequently, quantitative metrics, including SNR, PSNR, RMSE, and CC, were employed to further evaluate the performance.

SNR is a fundamental metric used to evaluate the quality of a signal by comparing the strength of the desired signal to the level of background noise. It is mathematically defined as

SNR =
$$10 \cdot \log_{10} \frac{\sum_{n=0}^{N-1} x_0^2(n)}{\sum_{n=0}^{N-1} [x_0(n) - y(n)]^2}$$
, (22)

where $x_0(n)$ is the original signal, y(n) is the denoised signal, and N is the total number of samples. A higher SNR value generally indicates a cleaner signal with less noise interference, which is often desirable in

applications such as medical imaging and SHM.

For a more nuanced assessment of signal quality, PSNR is commonly employed. This metric is based on the mean squared error (MSE) between the original and denoised signals:

$$PSNR = 10 \cdot \log_{10} \frac{\max(x_0^2(n))}{MSE}$$
 (23)

The MSE is calculated as

$$MSE = \frac{1}{N} \sum_{n=0}^{N-1} \left[x_0(n) - y(n) \right]^2$$
 (24)

Higher PSNR values indicate a closer match between the denoised and original signals, suggesting better preservation of signal integrity.

Another widely recognized metric is RMSE, which quantifies the average magnitude of differences between the original and denoised signals. It is expressed as:

RMSE =
$$\sqrt{\text{MSE}} = \sqrt{\frac{1}{N} \sum_{n=0}^{N-1} [x_0(n) - y(n)]^2}$$
 (25)

Unlike SNR and PSNR, lower RMSE values are preferable, as they indicate that the denoised signal is closer to the original.

Last but not least, CC measures the degree of linear relationship between the original and denoised signals. It provides a statistical assessment of the relationship between the original and denoised signals:

$$CC = \frac{\sum_{n=1}^{N} [x_0(n) - \overline{x}_0(n)]^2 [y(n) - \overline{y}(n)]^2}{\sqrt{\sum_{n=1}^{N} [x_0(n) - \overline{x}_0(n)]^2} \sqrt{\sum_{i=1}^{N} [y(n) - \overline{y}(n)]^2}}$$
(26)

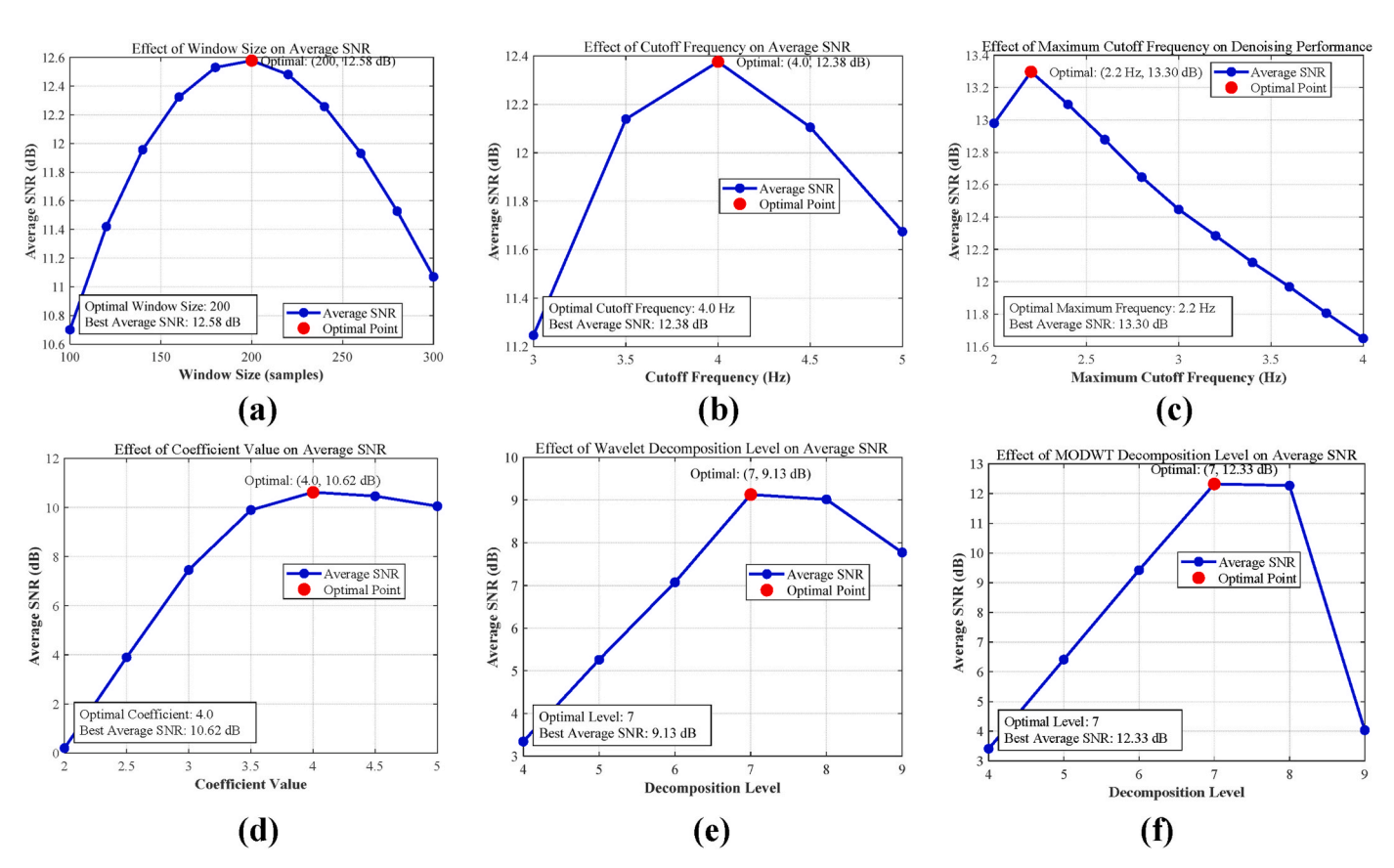


Fig. 5. Average SNR vs. hyperparameter search ranges for different denoising methods: (a) MA, (b) FIR, (c) FB, (d) FMD, (e) DWT, and (f) MODWT.

Table 3Key hyperparameters for the seven methods compared.

Dataset	Noisy data (I)	$MA(M_1)$	FIR (M_2, f_c)	EMD (l_c)	FB (f_{max})	FMD (<i>p</i>)	DWT (J_1)	MODWT (J_2)
1	0.1	50	100, 17	3	5.4	0.2	6	6
	0.5	90	100, 15	4	5.0	1	6	7
	1	120	500, 5	4	4.2	2	7	7
	3	200	500, 4	5	2.2	4	7	7
2	0.1	60	100, 4.6	3	5.6	0.2	7	6
	0.5	130	200, 4.6	5	2.4	1	7	7
	1	180	400, 3.8	5	1.8	2	7	7
	3	290	400, 2.6	6	1.4	4	8	8
3	0.1	60	100, 10.8	4	5.4	0.2	6	6
	0.5	160	200, 4.5	5	1.8	1.2	7	7
	1	210	400, 3.5	5	1.6	2.1	7	7
	3	350	400, 2.2	6	1.4	4	8	8

In this equation, $\overline{x}_0(n)$ and $\overline{y}(n)$ represent the mean values of the original and denoised signals, respectively. A CC close to 1 signifies a strong positive relationship, indicating that the denoised signal retains the structure of the original signal well. Conversely, a CC close to 0 implies little to no relationship between the signals, indicating a potential loss of information during the denoising process.

4. Results and discussions

The present study extensively investigates the denoising performance of various existing techniques. Three datasets, each comprising more than 200 strain signals, were used to synthesize noisy signals at four levels of noise intensity. Seven denoising methods were compared using all these noisy signals, totaling over 3000 instances.

The outputs from the seven compared denoising methods are illustrated in Fig. 6, which depicts samples of noisy signal with a noise

intensity ratio of 3.0 for each dataset. As detailed in subsection 3.2, the noisy signals were synthesized from each of the three datasets. The denoised images clearly demonstrate that the MODWT thresholding method outperforms the others across all three samples. It achieves effective denoising while preserving the signal's amplitude and maintaining the intricate features of the original signal.

In contrast, both the EMD and FMD methods exhibit relatively poor denoising performance, retaining a significant amount of residual noise and compromising some essential signal details, which results in a decreased amplitude of the strain signal. Furthermore, the application of FIR filters during denoising is susceptible to edge effects; for instance, severe edge effects can be observed when processing samples from Datasets 2 and 3. Although the DWT provides comprehensive denoising, it also removes critical details from the signal.

The MA and FB approaches yield comparatively better denoising results. However, due to constraints related to fixed windows or fixed

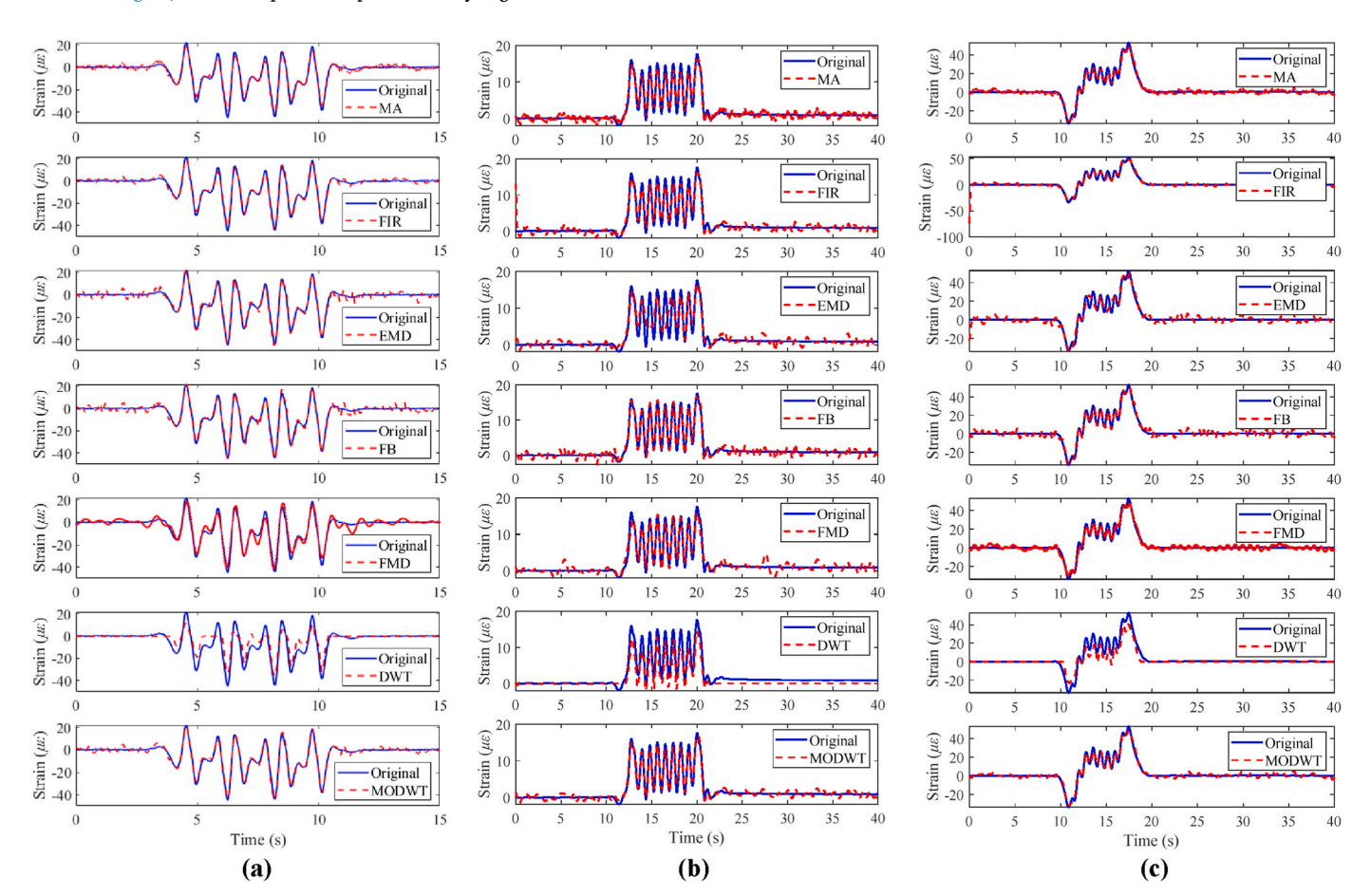


Fig. 6. Denoised strain signals using compared methods for samples from: (a) Database 1, (b) Database 2, and (c) Database 3.

frequency bands, these methods also exhibit considerable residual noise and may further diminish the detailed features of the signal.

The boxplots of the four quantitative metrics, i.e., SNR, PSNR, RMSE, and CC, to evaluate the denoising performance of the compared methods, are presented in Figs. 7–9. The mean values of these metrics are listed in Tables 4–7. These statistical plots and tables result from experiments conducted on noisy data at noise intensities of 0.1, 0.5, 1, and 3, synthesized from all signals in the three datasets listed in Table 1.

The MODWT thresholding method demonstrates excellent performance across all noisy signal datasets, consistently achieving superior performance metrics. The four metrics of this method reveal not only outstanding mean values but also smaller variances, as evidenced by the boxplots, indicating stable denoising performance. In contrast, the DWT thresholding method, also a wavelet approach, exhibits considerably inferior denoising performance when applied to these experimental signals. This discrepancy is highlighted by significant differences in performance metric values and their larger variability. In addressing complex signals, such as actual bridge strain, the downsampling employed by DWT to enhance computational efficiency may lead to a loss of critical information that cannot be overlooked. This limitation is particularly evident in Fig. 10, where the reduced number of coefficients in DWT obscures fine details and introduces noticeable edge effects at

signal boundaries, compared to the comprehensive and undistorted coefficient set provided by MODWT.

Further insight is gained from Fig. 11, which compares the coefficients used for signal reconstruction. Even when DWT and MODWT employ the same wavelet basis functions, the denoising performance of DWT reaches its optimal limit but remains suboptimal due to the inherent restrictions of its methodology, namely, the downsampling process that discards significant signal information. This loss compromises DWT's ability to accurately reconstruct the signal, especially in the presence of noise or abrupt changes typical of bridge strain data. Conversely, MODWT's elimination of downsampling ensures that all temporal information is retained, resulting in a more robust and accurate reconstruction of the original signal. This is reflected in the consistently lower variance and higher fidelity of the MODWT denoised outputs across Databases 1, 2, and 3.

The denoising performance of the EMD method also shows a significant gap. One contributing factor may be its susceptibility to mode mixing, which causes signals of varying frequencies to be combined within the resulting IMFs. Furthermore, its sensitivity to sharp discontinuities and nonlinearities, which are common characteristics of strain measurements, can result in distorted IMFs that fail to accurately represent the underlying signal.

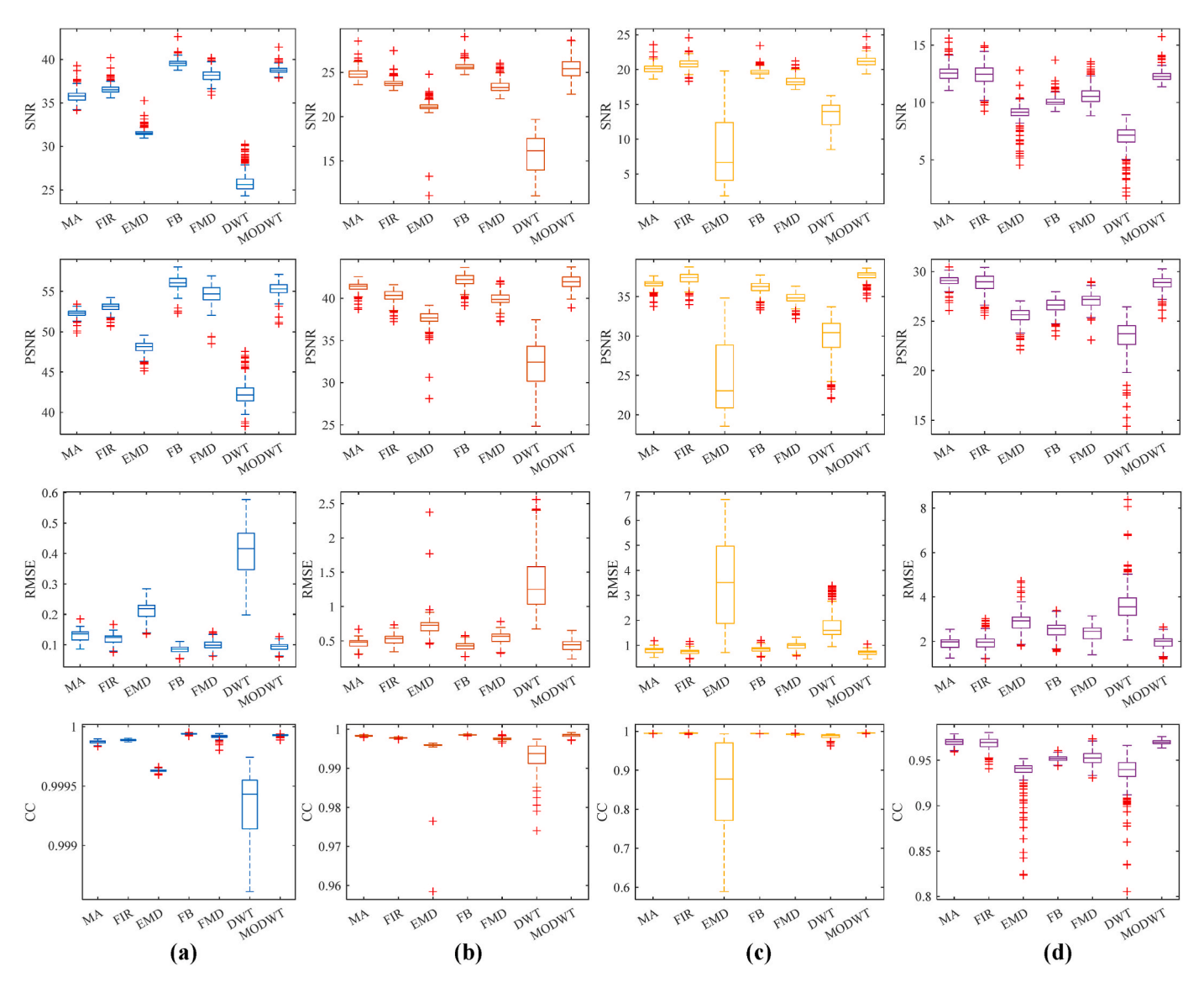


Fig. 7. Boxplots of denoising performance metrics for seven methods compared using Dataset 1: (a) I = 0.1, (b) I = 0.5, (c) I = 1.0, and (d) I = 3.0.

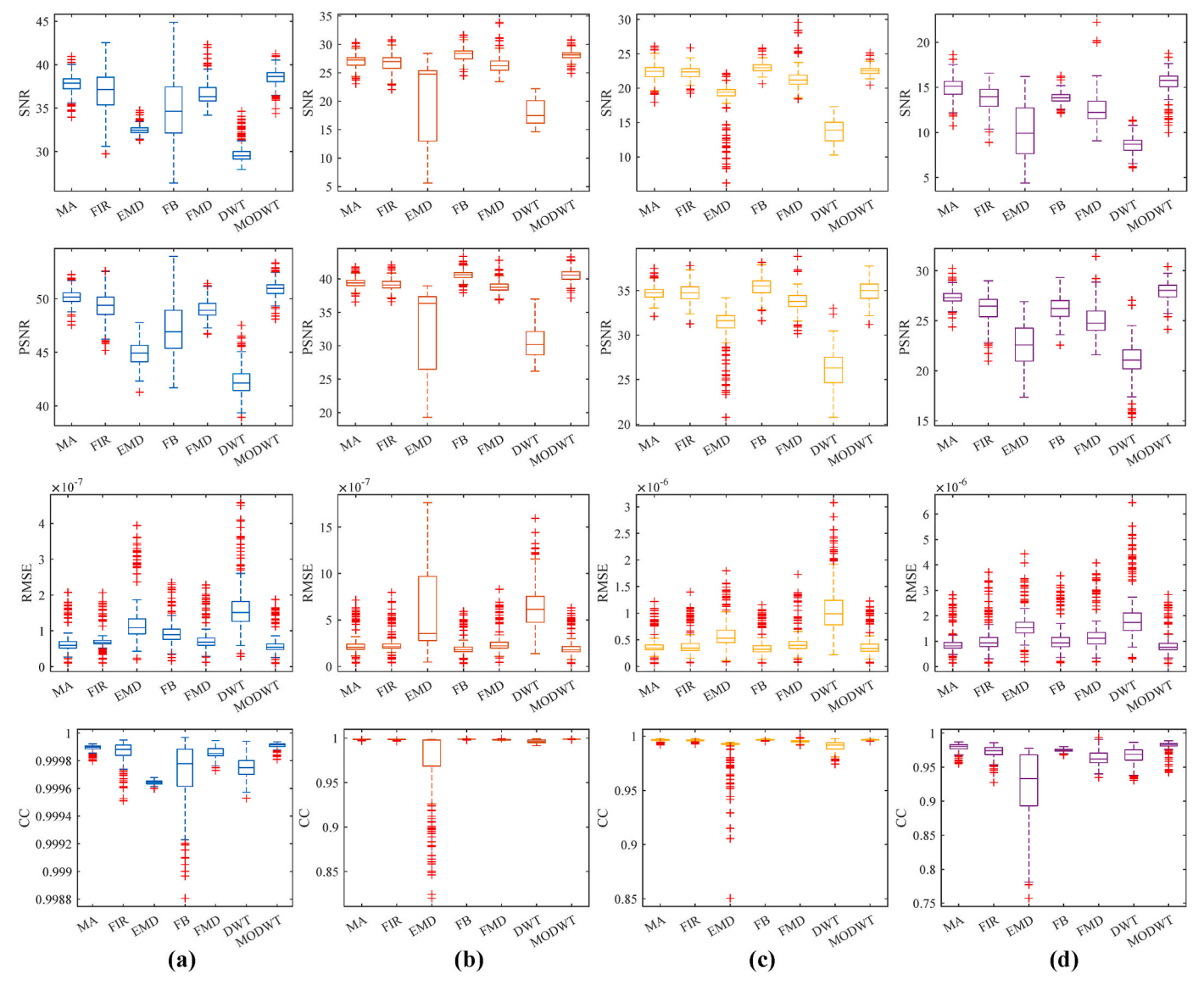


Fig. 8. Boxplots of denoising performance metrics for seven methods compared using Dataset 2: (a) I = 0.1, (b) I = 0.5, (c) I = 1.0, and (d) I = 3.0.

The two time-domain methods, MA and FIR, along with the two frequency-domain methods, FB and FMD, display commendable performance in denoising most noisy signal datasets; however, their overall performance lacks stability. In other words, while they may perform well on certain datasets, they can yield only ordinary results on others. Conversely, the MODWT method consistently maintains superior performance across all noisy signal datasets.

Based on the results presented, it can be concluded that among the methods compared for removing noise from strain signals collected from real bridges, the MODWT-based technique is the most effective, particularly under high noise conditions. This method preserves both the amplitude and pattern of the impulses, which reflect the static effects of vehicle weights crossing the bridge. This preservation is advantageous for more accurate structural condition assessments and improved decision-making regarding maintenance and repair strategies. For signals characterized by low noise levels, MA or FB filters also perform effectively. Therefore, in such cases, these two methods can be employed, especially as they are often computationally more efficient than MODWT. However, for signals containing strong or complex noise that is challenging to manage, the MODWT-based method is strongly recommended.

Regarding computational efficiency, MODWT requires more

processing time than other denoising methods for the same signal. To assess its suitability for real-time bridge SHM, we measured MODWT's computation time across the three datasets examined in this study. Fig. 12 presents boxplots of MODWT's processing times for denoising all signals in these datasets. Computations were performed on a PC with an Intel® Xeon® E5-1620 v4 CPU (3.50 GHz) and 16 GB RAM. Results show that MODWT processes signals of 40,000–50,000 points, sampled at 1000 Hz, in approximately 0.1 s. This means that 40 s of data are denoised in just 0.1 s, satisfying the real-time requirements of most bridge SHM applications.

5. Conclusions and future work

To address the challenges posed by non-stationary signals and broadband noise in bridge SHM, we conducted a comprehensive investigation on various techniques for denoising strain signals. Special attention was paid to MODWT, which excels in processing non-stationary and complex signals. Three datasets obtained from two different types of bridges were employed for this comparative study. Noisy signals with four different intensity levels were synthesized from these datasets. Seven representative denoising methods were compared using all these noisy signals. Both qualitative and quantitative

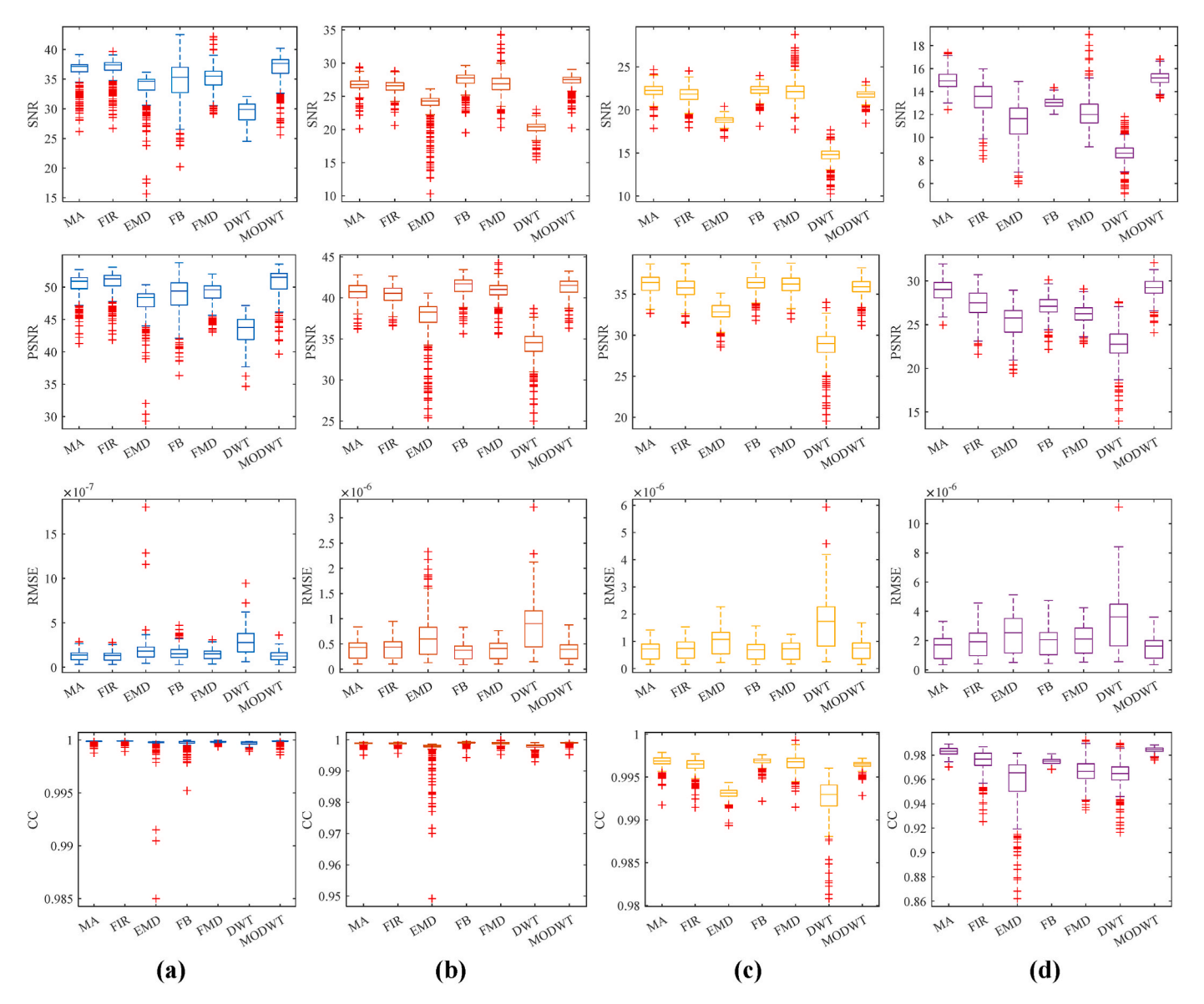


Fig. 9. Boxplots of denoising performance metrics for seven methods compared using Dataset 3: (a) I = 0.1, (b) I = 0.5, (c) I = 1.0, and (d) I = 3.0.

Table 4Comparison of mean SNR from different denoising methods.

Dataset	Noisy data (I)	MA	FIR	EMD	FB	FMD	DWT	MODWT
1	0.1	35.79	36.57	31.60	39.57	38.15	25.91	38.78
_	0.5	24.84	23.79	21.11	25.65	23.45	15.68	25.44
	1	20.12	20.79	8.57	19.68	18.35	13.33	21.18
	3	12.58	12.38	9.05	10.12	10.62	6.93	12.33
2	0.1	37.74	36.87	32.50	34.76	36.64	29.85	38.52
	0.5	26.99	26.73	20.27	28.20	26.41	18.04	28.11
	1	22.33	22.29	18.70	23.04	21.35	13.68	22.55
	3	14.96	13.79	10.09	13.83	12.61	8.57	15.52
3	0.1	36.31	36.67	33.55	34.53	35.04	29.35	36.61
	0.5	26.62	26.41	23.42	27.36	26.82	20.19	27.21
	1	22.23	21.69	18.79	22.27	22.14	14.73	21.76
	3	14.97	13.39	11.29	13.05	12.19	8.69	15.17

assessments were employed to evaluate the effectiveness of the methods being compared. The main conclusions can be drawn as follows.

- (1) Among the seven methods compared, MODWT proved to be the most effective in denoising the strain signals analyzed. In the graphical representation of the denoised signals, it preserves the
- signal's amplitude and maintains the intricate features of the original signal effectively. Furthermore, it consistently achieves superior performance metrics in terms of SNR, PSNR, RMSE, and CC.
- (2) Traditional methods, such as MA and FB filters, perform well in specific scenarios, particularly when the noise is low. Therefore,

Table 5Comparison of mean PSNR from different denoising methods.

Dataset	Noisy data (I)	MA	FIR	EMD	FB	FMD	DWT	MODWT
1	0.1	52.25	53.03	48.07	56.04	54.62	42.38	55.25
	0.5	41.31	40.26	37.58	42.12	39.92	32.15	41.90
	1	36.59	37.26	25.03	36.15	34.82	29.80	37.64
	3	29.04	28.84	25.52	26.58	27.08	23.40	28.79
2	0.1	50.15	49.27	44.90	47.17	49.05	42.25	50.93
	0.5	39.40	39.13	32.68	40.60	38.82	30.45	40.52
	1	34.74	34.69	31.10	35.44	33.76	26.09	34.96
	3	27.36	26.19	22.50	26.24	25.02	20.97	27.92
3	0.1	50.31	50.67	47.55	48.53	49.04	43.35	50.61
	0.5	40.62	40.41	37.42	41.36	40.82	34.19	41.21
	1	36.23	35.69	32.79	36.27	36.14	28.73	35.76
	3	28.97	27.39	25.29	27.05	26.19	22.69	29.17

Table 6Comparison of mean RMSE from different denoising methods.

Dataset	Noisy data (I)	MA	FIR	EMD	FB	FMD	DWT	MODWT
1	0.1	0.13	0.12	0.21	0.08	0.10	0.41	0.09
	0.5	0.46	0.52	0.71	0.42	0.54	1.36	0.43
	1	0.79	0.73	3.49	0.83	0.97	1.77	0.70
	3	1.88	1.93	2.83	2.49	2.36	3.64	1.93
2	0.1	6.83E-08	7.41E-08	1.27E-07	9.45E-08	7.69E-08	1.68E-07	6.24E-08
	0.5	2.35E-07	2.41E-07	6.08E-07	2.04E-07	2.51E-07	6.50E-07	2.08E-07
	1	4.02E-07	4.09E-07	6.18E-07	3.76E-07	4.60E-07	1.09E-06	3.99E-07
	3	9.38E-07	1.10E-06	1.62E-06	1.09E-06	1.26E-06	1.99E-06	8.87E-07
3	0.1	1.27E-07	1.22E-07	1.83E-07	1.60E-07	1.47E-07	2.81E-07	1.23E-07
	0.5	3.97E-07	4.06E-07	6.08E-07	3.61E-07	3.87E-07	8.46E-07	3.68E-07
	1	6.63E-07	7.06E-07	9.84E-07	6.56E-07	6.69E-07	1.61E-06	6.97E-07
	3	1.55E-06	1.85E-06	2.41E-06	1.91E-06	2.12E-06	3.25E-06	1.49E-06

Table 7Comparison of mean CC from different denoising methods.

Dataset	Noisy data (I)	MA	FIR	EMD	FB	FMD	DWT	MODWT
1	0.1	0.9999	0.9999	0.9996	0.9999	0.9999	0.9993	0.9999
	0.5	0.9983	0.9978	0.9957	0.9985	0.9976	0.9929	0.9984
	1	0.9950	0.9955	0.8577	0.9943	0.9921	0.9869	0.9959
	3	0.9702	0.9685	0.9370	0.9518	0.9527	0.9359	0.9700
2	0.1	0.9999	0.9999	0.9996	0.9997	0.9999	0.9998	0.9999
	0.5	0.9987	0.9986	0.9758	0.9990	0.9985	0.9964	0.9990
	1	0.9963	0.9962	0.9887	0.9969	0.9952	0.9908	0.9965
	3	0.9793	0.9726	0.9235	0.9749	0.9635	0.9668	0.9817
3	0.1	0.9999	0.9999	0.9996	0.9997	0.9998	0.9997	0.9999
	0.5	0.9988	0.9988	0.9967	0.9990	0.9988	0.9979	0.9990
	1	0.9968	0.9963	0.9931	0.9968	0.9966	0.9926	0.9965
	3	0.9829	0.9746	0.9579	0.9747	0.9664	0.9642	0.9841

under low-noise conditions, these methods can be considered effective denoising techniques, especially due to their straightforward algorithms.

(3) In cases where strong or complex noise is difficult to handle, the MODWT-based method is recommended. Unlike traditional techniques, MODWT does not involve downsampling, thus preserving all data points and significantly enhancing the resolution of both global and local signal features. Therefore, extensive experiments demonstrate that MODWT is stable and robust in effectively removing noise from all signals.

This research provides valuable insights into preprocessing techniques in SHM, which are essential for improved structural assessments and maintenance strategies. While we used Gaussian white noise to simulate noise in bridge strain signals, real-world conditions involve more complex noise profiles such as gradual baseline shifts from thermal expansion, pink noise (1/f noise) from material fatigue, impulse noise triggered by construction or lightning, and intrinsic sensor noise (e.g., thermal or quantization noise, calibration drift). To address this, our

future work will develop a more comprehensive noise model incorporating these mixed sources. We plan to collect extensive strain data across diverse conditions, such as seasonal temperature changes, electromagnetic interference, extreme weather, and high traffic, to validate MODWT and other preprocessing methods under realistic noises. We will also expand our dataset to include a broader range of bridge types (e.g., suspension, truss, arch, cable-stayed) to ensure robust performance under diverse scenarios. To bridge the gap between simulation and real-world deployment, we will explore the integration of these advanced preprocessing techniques into operational SHM systems. This will involve collaborating with bridge operators to conduct field tests, where the performance of our methods can be assessed under actual mixed noise conditions. These efforts will provide a more thorough understanding of the applicability and limitations of our approach, paving the way for more reliable and effective SHM solutions.

CRediT authorship contribution statement

Yun-Xia Xia: Writing - review & editing, Writing - original draft,

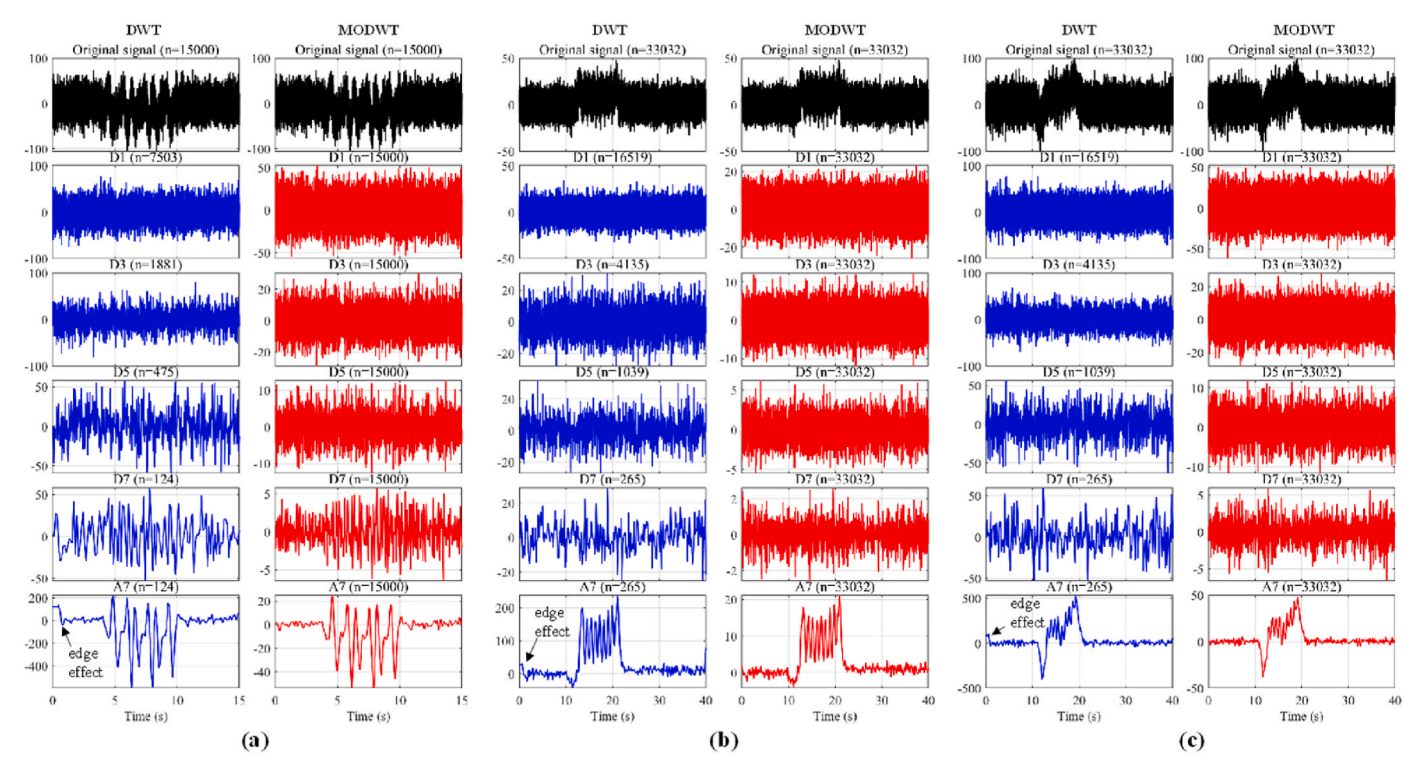


Fig. 10. Comparison of detail coefficients (Di) and approximation coefficients (Ai) obtained by DWT and MODWT for samples from: (a) Database 1, (b) Database 2, and (c) Database 3. Di and Ai represent the detail and approximation coefficients at level i.

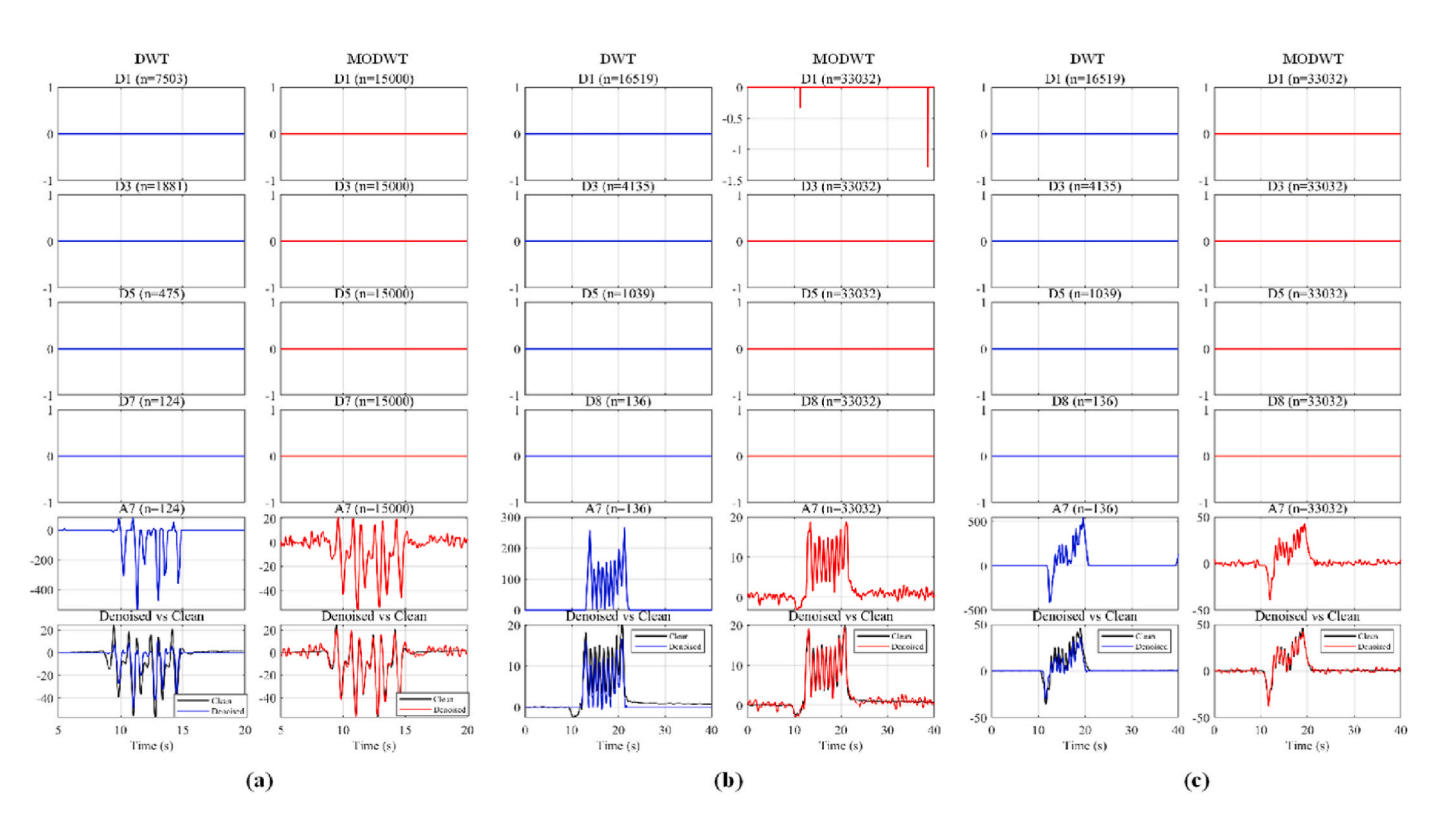


Fig. 11. Comparison of detail coefficients and approximation coefficients used by DWT and MODWT to reconstruct signals for samples from: (a) Database 1, (b) Database 2, and (c) Database 3.

Validation, Supervision, Methodology, Investigation, Funding acquisition, Formal analysis, Data curation, Conceptualization. Ru-Kai Xu: Visualization, Data curation. Yi-Qing Ni: Resources, Conceptualization. Zu-Quan Jin: Resources, Funding acquisition.

Declaration of competing interest

The authors declare that they have no known competing financial interests or personal relationships that could have appeared to influence

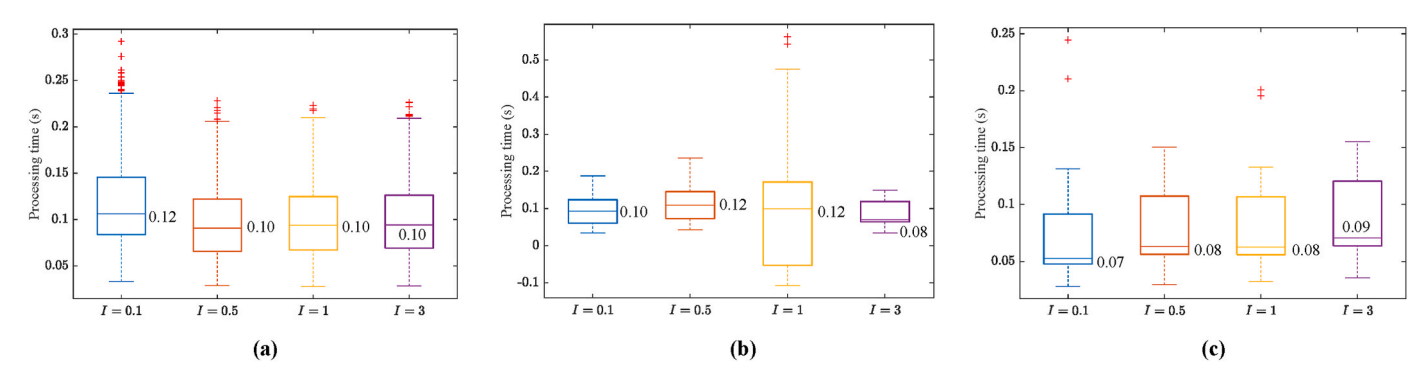


Fig. 12. Processing time of the MODWT method: (a) Dataset 1, (b) Dataset 2, and (c) Dataset 3.

the work reported in this paper.

The author Yi-Qing Ni is a Co-Editor-in-Chief for this journal and was not involved in the editorial review or the decision to publish this article.

Acknowledgements

This work is supported by the Natural Science Foundation of Shandong Province (Grant No. ZR2023ME105), and the National Natural Science Foundation of China (Grant Nos. 51708315 and U1806225). Comments and suggestions from the reviewers are appreciated very much.

References

Alexakis, H., Lau, F.D.H., DeJong, M.J., Research data supporting the publication, 2021. Fibre optic sensing of ageing railway infrastructure enhanced with statistical shape analysis. J. Civil Struct. Health Monit. 11, 49–67. https://doi.org/10.1007

Aliouat, M., Djendi, M., 2025. A new deep learning forward bss (d-fbss) algorithm for acoustic noise reduction and speech enhancement. Appl. Acoust. 230, 110413. https://doi.org/10.1016/j.apacoust.2024.110413.

Anastasopoulos, D., Roeck, G., Reynders, E., 2021. One-year operational modal analysis of a steel bridge from high-resolution macrostrain monitoring: influence of temperature vs. retrofitting. Mech. Syst. Signal Process. 161, 107951. https://doi.or g/10.1016/j.wpsp.2021.107951

Barzegar, R., Aalami, M., Adamowski, J., 2021. Coupling a hybrid cnn-lstm deep learning model with a boundary corrected maximal overlap discrete wavelet transform for multiscale lake water level forecasting. J. Hydrol. 598, 126196. https://doi.org/10. 1016/j.jhydrol.2021.126196

Blackledge, J.M., 2006. Digital Signal Processing: Mathematical and Computational Methods, Software Development and Applications, 2nd ed. Woodhead Publishing https://doi.org/10.1533/9780857099457.

Boashash, B., 2016. Time-frequency Signal Analysis and Processing: A Comprehensive Reference, 2nd ed. Academic press.

Bracewell, R.N., 2000. The Fourier Transform and its Applications, 3rd ed. McGraw-Hill. Cardoso, J.-F., 1998. Blind signal separation: statistical principles. Proc. IEEE 86 (10), 2009–2025. https://doi.org/10.1109/5.720250.

Comon, P., 1994. Independent component analysis, a new concept? Signal Process 36 (3), 287–314. https://doi.org/10.1016/0165-1684(94)90029-9.

Daubechies, I.. Ten Lectures on Wavelets. Society for Industrial and Applied Mathematics. https://doi.org/10.1137/1.9781611970104.

Deng, C., Li, Y., Zou, W., Ren, Y., Peng, Y., Han, Z., 2023. A de-noising algorithm for bridge cable force monitoring data based on mathematical morphology. Adv. Bridge Eng. 4, 28. https://doi.org/10.1186/s43251-023-00109-x.

Desjardins, S.L., Lau, D.T., 2024. Enhanced operational modal analysis and change point detection for vibration-based structural health monitoring of bridges. J. Infrastruct. Intell. Resil. 3 (4), 100121. https://doi.org/10.1016/j.iintel.2024.100121.

Donoho, D.L., Johnstone, I.M., 1994. Ideal spatial adaptation by wavelet shrinkage. Biometrika 81 (3), 425–455. https://doi.org/10.2307/2337118.

Dragomiretskiy, K., Zosso, D., 2013. Variational mode decomposition. IEEE Trans. Signal Process. 62 (3), 531–544. https://doi.org/10.1109/TSP.2013.2288675.

Glišić, B., 2024. Introduction to Strain-Based Structural Health Monitoring of Civil Structures. John Wiley & Sons, Ltd.. https://doi.org/10.1002/9781118700327

Hamming, R.W., 1989. Digital Filters, 3rd ed. Prentice Hall International (UK) Ltd. https://doi.org/10.5555/59853

Hu, W., Said, S., Rohrmann, R.G., Cunha, Á., Teng, J., 2017. Continuous dynamic monitoring of a prestressed concrete bridge based on strain, inclination and crack measurements over a 14-year span. Struct. Health Monit. 17 (5), 1073–1094. https://doi.org/10.1177/14550171.7735505

Huang, H., Yi, T., Li, H., Liu, H., 2020. Strain-based performance warning method for bridge main girders under variable operating conditions. J. Bridge Eng. 25 (4), 04020013. https://doi.org/10.1061/(ASCE)BE.1943-5592.0001538. Huang, N.E., Shen, Z., Long, S.R., Wu, M.C., Shih, H.H., Zheng, Q., Yen, N.-C., Tung, C.C., Liu, H.H., 1998. The empirical mode decomposition and the Hilbert spectrum for nonlinear and non-stationary time series analysis. Proc. R. Soc. Lond. A. 454, 903–995. http://doi.org/10.1098/rspa.1998.0193.

Hyvärinen, A., Hurri, J., Hoyer, P.O., 2009. Independent component analysis. Natural Image Statistics. Computational Imaging and Vision. Springer, London, pp. 151–175. https://doi.org/10.1007/978-1-84882-491-1_7.

Jiang, X., Lang, Q., Jing, Q., Wang, H., Chen, J., Ai, Q., 2022. An improved wavelet threshold denoising method for health monitoring data: a case study of the Hong Kong-Zhuhai-Macao bridge immersed tunnel. Appl. Sci. 12, 6743. https://doi.org/ 10.3390/app12136743.

Jiang, X., Wang, J., Shi, J., Shen, C., Huang, W., Zhu, Z., 2019. A coarse-to-fine decomposing strategy of VMD for extraction of weak repetitive transients in fault diagnosis of rotating machines. Mech. Syst. Signal Process. 116, 668–692. https:// doi.org/10.1016/j.ymssp.2018.07.014.

Kaur, C., Bisht, A., Singh, P., Joshi, G., 2021. EEG signal denoising using hybrid approach of variational mode decomposition and wavelets for depression. Biomed. Signal Process. Control 65, 102337. https://doi.org/10.1016/j.bspc.2020.102337.

Kopsinis, Y., McLaughlin, S., 2009. Development of EMD-based denoising methods inspired by wavelet thresholding. IEEE Trans. Signal Process. 57 (4), 1351–1362. https://doi.org/10.1109/tsp.2009.2013885.

Kumar, A., Tomar, H., Mehla, V.K., Komaragiri, R., Kumar, M., 2021. Stationary wavelet transform based ecg signal denoising method. ISA Trans 114, 251–262. https://doi. org/10.1016/j.isatra.2020.12.029.

Li, B., Zhang, Y., Liao, Z., Xue, Z., 2025. Bayesian mixture of factor analyzers for structural damage detection under varying environmental conditions. J. Infrastruct. Intell. Resil. 4 (2), 100140. https://doi.org/10.1016/j.iintel.2025.100140.

Li, C., Peng, J., Liang, M., 2014. Enhancement of the wear particle monitoring capability of oil debris sensors using a maximal overlap discrete wavelet transform with optimal decomposition depth. Sensors 14 (4), 6207–6228. https://doi.org /10.3390/s140406207.

Liashchynskyi, P., Liashchynskyi, P., 2019. Grid search, random search, genetic algorithm: a big comparison for NAS. arXiv 1912, 06059. https://doi.org/10.4855 0/arXiv.1912.06059.

Ma, J., Gong, Z., Yan, C., Cao, P., Wang, H., 2024. Wavelet denoising analysis on vacuum-process monitoring signals of aerospace vacuum vessel structures. Meas. Sci. Technol. 35, 126008. https://doi.org/10.1088/1361-6501/ad7481.

Maes, K., Lombaert, G.. Monitoring Data for Railway Bridge KW51 in Leuven, Belgium, before, during, and after Retrofitting (1.0). Zenodo. https://doi.org/10.5281/zenodoi.org/10.5281/z

Maes, K., Lombaert, G., 2021. Monitoring railway bridge KW51 before, during, and after retrofitting. J. Bridge Eng. 26 (3), 04721001. https://doi.org/10.1061/(ASCE)BE.19 43-5592.0001668.

Mao, J., Wang, H., Li, J., 2019. Fatigue reliability assessment of a long-span cable-stayed bridge based on one-year monitoring strain data. J. Bridge Eng. 24 (1), 05018015. https://doi.org/10.1061/(ASCE)BE.1943-5592.0001337.

Massar, H., Drissi, T.B., Nsiri, B., Miyara, M., 2025. Advancements in blind source separation for EEG artifact removal: a comparative analysis of variational mode decomposition and discrete wavelet transform approaches. Appl. Acoust. 228, 110300. https://doi.org/10.1016/j.apacoust.2024.110300.

Ni, Y., Xia, H., Wong, K.Y., Ko, J.M., 2012. In-service condition assessment of bridge deck using long-term monitoring data of strain response. J. Bridge Eng. 17 (6), 876–885. https://doi.org/10.1061/(ASCE)BE.1943-5592.0000321.

Oppenheim, A.V., Schafer, R.W., Buck, J.R., 1999. Discrete-time Signal Processing. 2nd ed. Prentice-Hall, Inc.

Oppenheim, A.V., Willsky, A.S., Nawab, S.H., 1997. Signals and Systms, 2nd ed. Prentice-Hall. Inc.

Osmani, S.A., Jun, C., Baik, J., Lee, J., Narimani, R., 2024. Wavelet-based precipitation preprocessing for improved drought forecasting: a machine learning approach using tunable Q-factor wavelet transform and maximal overlap discrete wavelet transform. Expert Syst. Appl. 257, 124962. https://doi.org/10.1016/j.eswa.2024.124962.

Patel, A.X., Kundu, P., Rubinov, M., Jones, P.S., Vértes, P.E., Ersche, K.D., Suckling, J., Bullmore, E.T., 2014. A wavelet method for modeling and despiking motion artifacts from resting-state fMRI time series. Neuroimage 95 (100), 287–304. https://doi. org/10.1016/j.neuroimage.2014.03.012.

- Percival, D.B., Walden, A.T., 2000. Wavelet Methods for Time Series Analysis. Cambridge University Press. https://doi.org/10.1017/CBO9780511841040.
- Pitas, I., Venetsanopoulos, A.N., 1990. Nonlinear Digital Filters: Principles and Applications. Springer, New York. https://doi.org/10.1007/978-1-4757-6017-0. Proakis, J.G., Manolakis, D.G., 2021. Digital Signal Processing: Principles Algorithms and

Applications, 5th ed. Pearson.

- Strang, G., Nguyen, T., 1996. Wavelets and Filter Banks. Wellesley-Cambridge Press. https://doi.org/10.1137/1.9780961408879. Sundararajan, D., 2015. Discrete Wavelet Transform: A Signal Processing Approach.
- John Wiley & Sons, Singapore Pte. Ltd. Tan, J., Chu, X., Cui, W., Zhao, L., 2024. Life-cycle assessment for flutter probability of a long-span suspension bridge based on operational monitoring data. J. Infrastruct. Intell. Resil. 3 (3), 100108. https://doi.org/10.1016/j.iintel.2024.100108
- Tian, C., Fei, L., Zheng, W., Xu, Y., Zuo, W., Lin, C., 2020. Deep learning on image denoising: an overview. Neural Netw 131, 251-275. https://doi.org/10.1016/j.
- Vaseghi, S.V., 2008. Advanced Digital Signal Processing and Noise Reduction. John Wiley & Sons, Ltd.
- Wahab, M.F., Gritti, F., O'Haver, T., 2021. Discrete fourier transform techniques for noise reduction and digital enhancement of analytical signals. TrAC, Trends Anal. Chem. 143, 116354. https://doi.org/10.1016/j.trac.2021.116354.

- Wei, S., Zhang, Z., Li, S., Li, H., 2017. Strain features and condition assessment of orthotropic steel deck cable-supported bridges subjected to vehicle loads by using dense FBG strain sensors. Smart Mater. Struct. 26 (10), 104007. https://doi.org/
- Wu, B., Li, Z., Chan, T., Wang, Y., 2014. Multiscale features and information extraction of online strain for long-span bridges. Smart Struct. Syst. 14 (4), 679-697. https://doi.
- Xia, Y.-X., Cheng, Y.-F., Ni, Y.-Q., Jin, Z.-Q., 2024. A data-driven wavelet filter for separating peak-shaped waveforms in SHM signals of civil structures. Mech. Syst. Signal Process. 219, 111588. https://doi.org/10.1016/j.ymssp.2024.111588.
- Yin, C., Wang, Y., Ma, G., Wang, Y., Sun, Y., He, Y., 2022. Weak fault feature extraction of rolling bearings based on improved ensemble noise-reconstructed EMD and adaptive threshold denoising. Mech. Syst. Signal Process. 171, 108834. https://doi. org/10.1016/j.ymssp.2022.108834.
- Yu, S., Ma, J., Wang, W., 2019. Deep learning for denoising. Geophysics 84 (6), V333-V350. https://doi.org/10.1190/geo2018-0668.1
- Zhao, H.-W., Ding, Y.-L., Nagarajaiah, S., Li, Ai-Q., 2019. Behavior analysis and early warning of girder deflections of a steel-truss arch railway bridge under the effects of temperature and trains: case study. J. Bridge Eng. 24 (1), 05018013. https://doi org/10.1061/(ASCE)BE.1943-5592.0001327.